PI-PI TO FULL CI: CATION DIMERS AND SUBSTITUENT EFFECTS IN NONCOVALENT INTERACTIONS

A Thesis
Presented to
The Academic Faculty

by

Stephen A. Arnstein

In Partial Fulfillment
of the Requirements for the Degree
Master of Science in
Chemistry

School of Chemistry and Biochemistry
Georgia Institute of Technology
May 2009

PI-PI TO FULL CI: CATION DIMERS AND SUBSTITUENT EFFECTS IN NONCOVALENT INTERACTIONS

Approved by:

Professor C. David Sherrill, Advisor
School of Chemistry and Biochemistry
Georgia Institute of Technology

Professor Jean-Luc Brédas
School of Chemistry and Biochemistry
Georgia Institute of Technology

Professor Joseph Perry
School of Chemistry and Biochemistry
Georgia Institute of Technology

Professor Nicholas V. Hud
School of Chemistry and Biochemistry
Georgia Institute of Technology

Date Approved: 8 January 2009

To my loving family and my late grandfather, John T. Richards Jr.

ACKNOWLEDGEMENTS

I would like to thank the members of the Center for Computational Molecular Science and Technology for their support over the past few years. I want to specifically acknowledge Professor Sherrill and Piotr Pieniazek for without them this thesis could not be possible. For moral support and many good times, I want to thank my many friends in the Chemistry Department at Georgia Tech. I would also like to Ed Hohenstein, Michael Marshall, Ashley Ringer, John Sears, Tait Dakota, Ashley Tucker and my other comrades in the office for many great times. Finally, I would like to thank the sources of funding for the projects that I have worked on at Georgia Tech: a presidential fellowship from Georgia Tech, a fellowship from the Center for Organic Photonics and Electronics (COPE) at Georgia Tech, a molecular biophysics training grant from Georgia Tech, the National Science Foundation (Grant No. CHE-0715268), the Petroleum Research Fund of the ACS (Grant No. 44262-AC6), the Center for Computational Molecular Science and Technology (NSF CRIF award CHE 04-43564), and the Chemistry Department at Georgia Tech.

TABLE OF CONTENTS

LIST OF TABLES

LIST OF FIGURES

SUMMARY

The following thesis focuses on two challenging areas of chemistry, π-π interactions and radical cation dimers. Approximations to the exact solution to the Schrödinger equation are investigated for these types of chemical systems with a variety of theoretical methods. The first chapter provides an introduction to the various quantum mechanical methods used in this research. The second chapter focuses specifically on π-π interaction. In this chapter, high quality quantum mechanical methods are used to examine how substituents tune π-π interactions between monosubstituted benzene dimers in parallel-displaced geometries. In addition, the role of dispersion and coulombic interactions in these systems is investigated to determine the nature of the substituent effect. In the third chapter radical cation dimers are investigated. Benchmark results with full configuration interaction (FCI) and equation-of-motion coupled-cluster for ionized systems (EOM-IP-CCSD) are presented for prototypical charge transfer species. Conclusions regarding chapters 2 and 3 are presented in the final chapter. This work may form the basis for improved approaches to rational drug design, organic optical materials, and molecular electronics.

CHAPTER I

INTRODUCTION

Radical cation dimers and π-π interactions are interesting but challenging to study. Numerous chemical and biochemical systems contain π-π interactions. All nucleic acids and several amino acids have the ability to form π-π complexes. These systems are difficult to study because the explicit interaction between electrons (rather than an averaged or effective interaction) is necessary to obtain an accurate model. Radical cations are interesting because of their importance in fundamental processes such as charge transfer. These systems are challenging because routine methods fail to describe near degeneracy of electron configurations. In this thesis, high accuracy quantum mechanical methods are used to study these systems.

Many questions in chemistry are not easily answered with experiment alone. The development of quantum mechanics and its incorporation into chemistry has diversified the chemist's tool box for solving scientific questions. A variety of theoretical methods exist. Classical mechanical approaches such as molecular mechanics describe atoms in molecules as charged spheres connected by harmonic springs. These classical methods are capable of describing a variety of systems; however, they do not explicitly describe electrons. Therefore, classical methods can not be used to describe dispersion, the instantaneous rearrangement of electrons; charge transfer; or radical systems because standard classical methods are not parametrized to describe an unpaired electron. This thesis will focus on quantum mechanical approaches for describing electrons explicitly.

In quantum mechanics, the state of a chemical system is defined by its wavefunction. The energy of a specific state can be obtained by the famous Schrödinger

equation:

$$\mathbf{H}\Psi = E\Psi. \tag{1}$$

In this equation $\mathbf{H}$ represents the Hamiltonian of the system, Ψ represents the wavefunction and E is the energy of the system. In quantum chemistry, the Hamiltonian represents the electrons and nuclei of a molecular system, shown in equation (2).

$$\mathbf{H} = -\overbrace{\sum_i \frac{1}{2}\nabla_i^2}^{(a)} - \overbrace{\sum_{iA} \frac{Z_A}{r_{iA}}}^{(b)} + \overbrace{\sum_{ij} \frac{1}{r_{ij}}}^{(c)} + \overbrace{\sum_{AB} \frac{Z_A Z_B}{R_{AB}}}^{(d)} - \overbrace{\sum_A \frac{1}{2M_A}\nabla_A^2}^{(e)} \tag{2}$$

In the Hamiltonian above, i and j represent electrons and A and B represent nuclei. The summations are (a) the kinetic energy of the electrons, (b) the coulombic interaction between electrons and nuclei, (c) the coulombic interaction between two electrons, (d) the coulombic interaction between two nuclei and (e) the kinetic energy of the nuclei. After applying the Born-Oppenheimer Approximation, which assumes that the electrons are moving much faster than the nuclei and the nuclei are stationary relative to the electrons, the nuclear kinetic energy (e) becomes zero and the nuclear repulsion energy (d) is a constant for any given configuration of nuclei.

If the Born-Oppenheimer approximation is used, an exact solution to the Schrödinger equation is possible for one electron systems, such as the hydrogen atom, H_2^+, He^+, Li^{2+}, etc. The solution of the wavefunction for a hydrogen-like atom leads to a series of functions with the form shown in equation (3). In the case of the hydrogen atom, the one-electron wavefunctions are the atomic orbitals. The exact form of the wavefunction depends on the state of the system which can be specified by the quantum numbers n, l, and m. The first term in equation (3) is the radial function and the second term is the spherical harmonic function. The radial function always has a $e^{-\zeta r}$ term, where ζ is a constant proportional to the charge of the nucleus of the atom.

$$\Psi_{n,l,m}(r,\theta,\phi) = R_{n,l}(r)Y_{l,m}(\theta,\phi) \tag{3}$$

For polyelectronic systems the exact solution to the wavefunction is unattainable. Slater orbitals were first used to approximate orbitals of atoms. They have the form shown in (4). In this equation, N is the normalization constant, $Y_{l,m}$ is the spherical harmonic function and ζ is a parameter.

$$\Psi_{\zeta,n,l,m}(r,\theta,\phi) = NY_{l,m}(\theta,\phi)r^{n-1}e^{-\zeta r} \tag{4}$$

Slater orbitals are inefficient for quantum chemistry calculations because the three- and four-center two-electron integrals cannot be computed analytically.[54] These integrals arise from the electron-electron repulsion term in the Hamiltonian. A single Slater orbital can be approximated by a linear combination of Gaussian functions. Although more functions are involved, the calculation is faster because the Gaussian product theorem allows for the solution of four-centered electron repulsion integrals to be calculated analytically. In spherical coordinates, the Gaussian type orbitals (GTOs) take on the form shown in equation (5). The GTOs can also be written in Cartesian coordinates as shown in equation (6).[54]

$$\Psi_{\zeta,n,l,m}(r,\theta,\phi) = NY_{l,m}(\theta,\phi)r^{(2n-2-l)}e^{-\zeta r^2} \tag{5}$$

$$\Psi_{\zeta,l_x,l_y,l_z}(x,y,z) = Nx^{l_x}y^{l_y}z^{l_z}e^{-\zeta r^2} \tag{6}$$

Some of the first basis sets developed for quantum chemistry were called STO-nG. In these Slater Type Orbitals (STOs), n represents the number of contracted Gaussian functions used to approximate a Slater orbital. For example, STO-3G has three Gaussian functions that are summed (or contracted) to represent one function for each orbital. The name is somewhat a misnomer, because the functions in the

basis set are actually Gaussian functions not Slater functions. These basis sets are also know as minimal basis sets, because they contain a single STO for each occupied orbital in the molecule. Other basis sets add additional orbitals on each atom and allow for a greater amount of flexibility in the wavefunction.

Other basis sets have been developed by Pople, Dunning, and others. The Pople style basis sets have the general form *a*-*bcd*+G(d,p). In this basis set, the *a* represents the number of primitive Gaussian functions used for each core orbital, and *b*, *c* and *d* represent the number of contracted Gaussian functions used for each valence orbital. The + sign signifies the addition of a set of diffuse s and p functions on heavy atoms, i.e. atoms other than hydrogen, and (d,p) represent polarization functions. Specifically, (d,p) adds higher *d*-angular momentum functions on heavy atoms and *p*-angular momentum functions on hydrogen atoms.

A minimal basis set does not describe the molecular orbitals well enough. Split valence basis sets allow a better description of valence orbitals that are involved in bonding. These basis sets describe core orbitals with a single linear combination of Gaussian functions (with fixed weights), but describe valence orbitals as a combination of sets of Gaussian basis functions. This allows the orbitals involved in bonding to better adapt to their electronic environment. Adding more basis functions to the valence orbitals is not always enough to obtain an good approximation to the wavefunction. As a classic example, ammonia will optimize to a more planar than trigonal pyramidal structure if additional polarization functions are not added to the basis set.[31] Higher angular momentum polarization functions on the nitrogen provide the system with enough flexibility to mimic the lone pair orbital above the nitrogen atom and an SO^3 character of the atomic bonding. Diffuse functions have been found to be critical in appropriately modeling anions and noncovalently bonded systems.

Dunning style basis sets have the general form aug-cc-pV*N*Z. The *N* represents the number of split valences in the basis set. *N* can take on values of D (double), T

(triple), Q (quadruple), 5, 6, etc. Each time another set of orbitals and an additional set of higher angular momentum functions are added to the basis set. The aug prefix denotes an additional set of diffuse orbitals of each angular momentum in the basis set.

In quantum chemistry, a level of theory must be selected. A level of theory consists of a method and a basis sets. It is important that the level of theory accurately describes the problem being studied. This is done by choosing a method with the appropriate physics for the problem and a basis set that is flexible enough to accurately describe the wavefunction of the system.

The exact solution to the Schrödinger equation cannot be obtained for systems with more than one electron. However, Hartree-Fock theory provides a method for approximating the energy of a molecule by neglecting the instantaneous interaction of two electrons. In Hartree-Fock theory the wavefunction is constructed from a set of basis functions and a Slater determinant. An example Slater determinant for an N electron system is shown in equation (7). In this equation, $\chi_i(n)$ represents the position of electron n in molecular orbital i. The molecular orbitals are functions that describe the position of electrons in a molecule.

$$\Psi(1,2,\ldots,N) = \begin{vmatrix} \chi_1(1) & \chi_2(1) & \cdots & \chi_N(1) \\ \chi_1(2) & \chi_2(2) & \cdots & \chi_N(2) \\ \cdots & \cdots & \ddots & \cdots \\ \chi_1(N) & \chi_2(N) & \cdots & \chi_N(N) \end{vmatrix} \tag{7}$$

The determinant is a convenient way of expressing the wavefunction as a sum of the products of the molecular orbitals. Expressing the wavefunction in this way requires it to obey the antisymmetry principle of quantum mechanics. An example two-electron wavefunction is shown in equation (8). Swapping electron one and two changes the sign of the wavefunction, as should occur for fermions.

$$\Psi(1,2) = \begin{vmatrix} \chi_1(1) & \chi_2(1) \\ \chi_1(2) & \chi_2(2) \end{vmatrix} = \chi_1(1)\chi_2(2) - \chi_2(1)\chi_1(2) \tag{8}$$

As shown in equation (9), the molecular orbitals (χ) are formed from a linear combination of basis functions (ϕ_μ) in the basis set. Roothaan showed that this representation of the orbitals generates a set of algebraic equations that can be solved using matrix algebra.[132] The coefficients, $c_{\mu i}$, are optimized to find the lowest energy solution.

$$\chi_i = \sum_\mu c_{\mu i}\phi_\mu \tag{9}$$

The variational theorem, shown in equation (10), states that if a normalized trial wavefunction, $\tilde{\Phi}$ is used, then the expectation value of the Hamiltonian is always greater than or equal to the true ground state energy.

$$\langle\tilde{\Phi}|H|\tilde{\Phi}\rangle \geq E_0 \tag{10}$$

In Hartree-Fock Theory, the solution to the energy is determined by arriving at a self-consistent field solution. The major approximation of the Hartree-Fock method is that each electron only feels the average field of all the other electrons. The instantaneous interaction between two electrons is not considered, and the movement of electrons is not correlated. Therefore, Hartree-Fock theory does not describe the phenomenon of dispersion. Other methods in quantum chemistry aim at improving upon Hartree-Fock theory by providing a better description of the correlation energy.

Perturbation theory can be used to improve upon Hartree-Fock theory. One of the more common methods is second order Møller-Plesset perturbation theory (MP2). The drawback to increased accuracy is increased computational cost. Hartree-Fock theory formally scales as O(N^4), whereas, MP2 theory scales as O(N^5).

The Hamiltonian used in perturbation theory is a sum of a zeroth-order Hamiltonian (H_0) and a parameter (λ) times a perturbation operator (V), shown in equation (11). The wavefunction and the energy become a summation, as shown in equations (12) and (13) respectively.

$$H = H_0 + \lambda V \tag{11}$$

$$\Psi_i = \Psi_i^{(0)} + \lambda\Psi_i^{(1)} + \lambda^2\Psi_i^{(2)} + \cdots = \sum_{n=0} \lambda^n \Psi_i^{(n)} \tag{12}$$

$$E_i = E_i^{(0)} + \lambda E_i^{(1)} + \lambda^2 E_i^{(2)} + \cdots = \sum_{n=0} \lambda^n E_i^{(n)} \tag{13}$$

The parameter λ formally ranges from 0 to 1 but in practice is set to 1. The perturbation operator is the difference between the Hartree-Fock Hamiltonian and the exact Hamiltonian. The sum of the zeroth and first order energy is the Hartree-Fock energy. Improvement on Hartree-Fock theory is obtained when the second order energy is included. The second order energy is shown in equation (14). The wavefunction Ψ_{ab}^{rs} represents double excitations, or promotion of electrons from occupied orbitals a and b to unoccupied orbitals r and s.

$$E_0^{(2)} = \sum_{a<b,r<s} \frac{|\langle\Psi_0|\sum_{i<j}\frac{1}{r_{ij}}|\Psi_{ab}^{rs}\rangle|^2}{\epsilon_a + \epsilon_b - \epsilon_r - \epsilon_s} \tag{14}$$

Perturbation theory is an improvement on Hartree-Fock theory, however, it is not without its own flaws. Including corrections greater than second order does not guarantee greater accuracy, because Møller-Plesset theory is not a variational method. In addition, MP2 will fail if there are near degeneracies in the molecular orbitals. By looking at the denominator in equation (14) one can see that if the sum of the eigenvalues of ϵ_a and ϵ_b is equal to the sum of the eigenvalues ϵ_r and ϵ_s, then the equation is undefined due to division by zero. MP2 theory is known to fail

due to degeneracies and multireference character of the system. Bond breaking is an example where more than one reference state is required to properly describe the system. This multireference character of the system occurs because orbitals become nearly degenerate.

One way to improve upon perturbation theory is with configuration interaction (CI). In configuration interaction, the wavefunction is expressed as a linear combination of Slater determinants. The general CI wavefunction is shown in equation (15). In this equation Φ_{SCF} is the original Hartree-Fock Slater determinant. The other determinants Φ_N are formed from exciting electrons from occupied orbitals to unoccupied orbitals to form a different electronic configuration. For example, Φ_S is a Slater determinant with a single electron moved from an occupied orbital in the reference wavefunction (Φ_{SCF}) to an unoccupied orbital, Φ_D represents a double excitation or the simultaneous excitation of two electrons from occupied orbitals to unoccupied orbitals, Φ_T is a triple excitation, and so on.

$$\Psi_{CI} = a_0 \Phi_{SCF} + \sum_S a_S \Phi_S + \sum_D a_D \Phi_D + \sum_T a_T \Phi_T + \cdots \tag{15}$$

Full configuration interaction (Full CI) includes all possible electronic configurations or Slater determinants for a given set of molecular orbitals. Although the exact solution to the Schrödinger equation can only be determined for one electron systems, full CI provides the exact solution to any N-electron wavefunction within a given basis set. If an appropriate basis set is used, then full CI is the most accurate method in quantum chemistry. The problem is full CI is only possible for small systems and small basis sets. Increasing the number of electrons or valence orbitals greatly increases the computational cost. Full CI scales factorially with respect to system size.

One can achieve better scaling if the number of configurations is truncated. Any of the configurations can be included, but typically the wavefunction is truncated

at some order of excitation. For example, CID would include only the reference determinant and all doubly excited determinants; whereas, CISD includes all singly and doubly excited determinants. Truncation from full CI to CISD greatly decrease the scaling of the method from $O(N!)$ to $O(N^6)$. The main flaw in truncation of the CI wavefunction is the method is no longer size-extensive or size-consistent.

For a method to be size-extensive, the energy of system should scale linearly with the number of particles. A size-consistent method is one where the sum of the energy of two non-interacting particles is the same as the energy of including both particles in the same calculation. For example a size-consistent method, the energy of n non-interacting water molecules is equal to n times the energy of a single water molecule.

Configuration interaction scales poorly with respect to system size and suffers from the being neither size-consistent or size-extensive. Coupled cluster (CC) theory is a method that is both size-consistent and size-extensive. More importantly, coupled cluster theory can achieve increased accuracy at similar cost to configuration interaction for a given excitation order.

In coupled cluster theory, equation (16), an exponential operator generates excited determinants from a reference wavefunction (Ψ_0). The reference wavefunction is often the original Hartree-Fock wavefunction. The operator $\mathbf{T}$ is a sum of excitation operators $\mathbf{T}_N$, equation (17). The $\mathbf{T_1}$ operator acts on the reference wavefunction to form singly excited determinants Φ_i^a (where the electron in orbital i is promoted to orbital a) multiplied by the coefficient t_i^a. This is analogous to the singly excited determinants Φ_S in configuration interaction. Similarly, $\mathbf{T_2}$ acts on the reference wavefunction to form double excited determinants Φ_{ij}^{ab} multiplied by the coefficient t_{ij}^a, as shown in equation (19).

$$\mathbf{H}e^{\mathbf{T}}\Psi_0 = E_{CC}\Psi_{CC} \tag{16}$$

$$\mathbf{T} = \mathbf{T_1} + \mathbf{T_2} + \mathbf{T_3} + \cdots + \mathbf{T_N} \tag{17}$$

$$\mathbf{T}_1\Phi_0 = \sum_{i}^{occ}\sum_{a}^{vir} t_i^a \Phi_i^a \tag{18}$$

$$\mathbf{T}_2\Phi_0 = \sum_{i<j}^{occ}\sum_{a<b}^{vir} t_{ij}^{ab} \Phi_{ij}^{ab} \tag{19}$$

A Taylor series expansion can be used to represent the exponential operator as an infinite sum, equation (20). The $\mathbf{T}$ operator, equation (17), is substituted into this infinite sum and terms are collected based on there order of excitation as shown in equation (21). The term $(\mathbf{T}_2 + \frac{1}{2}\mathbf{T}_1^2)$ is the sum of true connected double excitation and the product of two single disconnected excitation. The term disconnected refers to the fact that the two single excited electrons are non-interacting.

$$e^{\mathbf{T}} = \mathbf{1} + \mathbf{T} + \frac{1}{2}\mathbf{T}^2 + \frac{1}{6}\mathbf{T}^3 + \cdots \tag{20}$$

$$e^{\mathbf{T}} = \mathbf{1} + \mathbf{T}_1 + (\mathbf{T}_2 + \frac{1}{2}\mathbf{T}_1^2) + (\mathbf{T}_3 + \mathbf{T}_2\mathbf{T}_1 + \frac{1}{6}\mathbf{T}_1^3) + \cdots \tag{21}$$

In the limit that all possible excitations are included coupled cluster theory is equivalent to full configuration interaction. However this is only feasible for small systems. Therefore, the $\mathbf{T}$ operator is typically truncated at some order of N. For example, if the operator is truncated at $T_1 + T_2$, then the method is coupled cluster with single and double excitations (CCSD). The truncated exponential operator is shown in equation (22).

$$e^{\mathbf{T}_1+\mathbf{T}_2} = \mathbf{1} + \mathbf{T}_1 + (\mathbf{T}_2 + \frac{1}{2}\mathbf{T}_1^2) + (\mathbf{T}_2\mathbf{T}_1 + \frac{1}{6}\mathbf{T}_1^3) + \cdots \tag{22}$$

CCSD formally scales the same of CISD as $O(N^6)$; however, CCSD is more accurate because higher-order excitations are introduced by the product of lower excitations. These states do not appear in configuration interaction and are considered disconnected excitations. For example, quadruple excitations are included through the product of two double excitation operators, even though there are no explicit quadruples parameters to solve for. In addition, truncated coupled cluster theory does not suffer from the size-extensive problem of truncated configuration interaction.

In many chemical systems, the correlation energy is not converged by including only singly and doubly excited determinants. For these cases, triple and higher-order excitations need to be included. CCSD with perturbative triples, CCSD(T), is referred to in the literature as the gold standard of quantum chemistry. The CCSD(T) method uses perturbation theory to approximate the triple excitations. The triples step of the calculation scales as $O(N^7)$

Over the next two following chapters, noncovalent ionized dimers and substituent effects in parallel displaced π-π interactions will be discussed. The work in the next chapter has been previously published in the journal Physical Chemistry Chemical Physics.[6] In this chapter high quality quantum mechanical methods, including CCSD(T) are used to examine how substituents tune π-π interactions between monosubstituted benzene dimers in parallel-displaced geometries. In the following chapter, benchmark full configuration interaction (FCI) and equation-of-motion coupled-cluster model with single and double substitutions for ionized systems (EOM-IP-CCSD) results are presented for prototypical charge transfer species. This work has been previously published in the Journal of Chemical Physics.[95]

CHAPTER II

SUBSTITUENT EFFECTS IN PARALLEL-DISPLACED π-π INTERACTIONS

Noncovalent π-π interactions are of fundamental importance for understanding chemical and biochemical systems.[83] These types of interactions are of biological importance in protein side-chain interactions,[14] nucleobase stacking,[110] and drug intercalation in DNA and RNA.[113] In addition, π-π interactions are found in organic crystals[24] and organic semiconductors.[105] Much of the theoretical work on understanding the nature of π-π interactions has focused on the benzene dimer.[50,53,119,121,122,127,134–136] A limited number of experimental and theoretical studies have gone on to examine how substituents may tune π-π interactions. These studies have focused primarily on substituent effects in edge-to-face (T-shaped) and face-to-face (sandwich) configurations.[2,17,25–27,59,68,93,97,102,103,118,120] Even fewer studies have focused on substituent effects in parallel-displaced configurations.[21,22,46,69,99,133]

Of the studies concerned primarily with parallel-displaced configurations, Hunter and co-workers studied substituent effects on the free energies of interaction of molecular zipper complexes using the double mutant cycle method.[21,22] That study evaluated the $\Delta\Delta$G of 24 different aromatic stacking interactions in a fixed geometry. The authors concluded that the electrostatic nature of the ring dominates the interaction energy, but that direct electrostatic interactions between substituents are also important. In another study by Rashkin and Waters, substituent effects in offset π-π interactions were observed by comparing rotational barriers in *N*-benzyl-2-(2-fluorophenyl)-pyridinium bromides using NMR techniques.[99] The authors observed that the electron-withdrawing substituents increase the magnitude of the rotational

barrier and propose that this is due to a decreased electron density of the π-clouds, leading to a reduced electrostatic repulsion between the negatively charged π-clouds. This finding appears to be consistent with NMR experiments on syn/anti conformers of substituted triptycene derivatives carried out by Gung et al.[47] It should be noted that Rashkin and Waters also observed an increased rotational barrier in meta-substituents versus para-substituents and proposed that this is due to interactions between the substituent and hydrogen atoms on the other ring.

Gung and Amicangelo have studied substituent effects in complexes of hexafluorobenzene with benzene using the MP2/fug-cc-pVDZ level of theory.[46] They observed that the complex binds more strongly when the substituent on benzene is displaced away from the hexafluorobenzene ring, rather than on top of the ring. A parallel displaced orientation was also found to be a minimum in the benzene-hexafluorobenzene complex, in contrast to the sandwich structure that might be expected considering only electrostatics. The authors concluded that electron donating groups on benzene increase the interaction energy in benzene-hexafluorobenzene, whereas electron-withdrawing groups decrease the interaction energy. The authors noted that electrostatic effects are very significant but are not the only cause for binding in these complexes.

A recent study by Kim, Hobza, and co-workers has examined aromatic interactions in substituted benzene-benzene systems.[69] The study compares geometries and single point energy computations with the CCSD(T) method. Their study concludes that substituents tend to increase the stability of displaced stacked structures over the T-shaped configurations. In contrast to the substituted benzene-hexafluorobenzene study of Gung and Amicangelo,[46] the substituted benzene complexes considered have an enhanced binding regardless of the electron donating nature of the substituent. In addition, these authors conclude that the dispersion and exchange-repulsion mostly cancel at equilibrium geometries and that electrostatics are the dominant contribution

to the relative energy.

While previous studies have focused on geometries and energies near the optimum intermolecular distances, the present work seeks to understand how substituents tune π-π interactions in parallel-displaced configurations across entire potential energy curves. This is particularly relevant for better understanding complex biochemical systems, where competing interactions or steric constraints may prevent a particular π-π interaction from achieving what would be the ideal geometry in an isolated bimolecular complex (see also the recent work of Bickelhaupt and co-workers[131] for a study of interaction energies in stacked nucleobases as a function of twist angle). While we present quantitatively reliable potential energies in the course of our study, the emphasis is on an understanding of how parallel-displaced π-π interactions are best understood qualitatively. We also examine both how a substituent affects the ring-ring interactions, as well as how a substituent interacts directly with another ring. Results are analyzed in terms of fundamental electrostatic, exchange-repulsion, induction, and dispersion interactions with the aid of symmetry-adapted perturbation theory.[55]

2.1 Theoretical Methods

Computations were performed using Dunning's augmented correlation-consistent polarized valence basis sets of double-ζ (aug-cc-pVDZ) and triple-ζ (aug-cc-pVTZ) quality.[58] The aug prefix denotes the addition of a set of diffuse functions for each angular momentum in the basis set. For brevity, we will often refer to the aug-cc-pVXZ results by the shorthand notation AXZ. In addition to the standard augmented basis sets, we employed a truncated aug-cc-pVDZ basis, denoted aug-cc-pVDZ′, which removes diffuse functions from hydrogen and diffuse *d* functions from all heavier atoms. The smaller aug-cc-pVDZ′ basis set was helpful in making the symmetry-adapted perturbation theory (SAPT)[55,143] computations more tractable.

Second-order Møller-Plesset perturbation theory (MP2) was used initially to scan the potential energy surface of all systems studied. High level coupled-cluster theory with single and double excitations and perturbative treatment of triples [CCSD(T)][98] was used where feasible to obtain highly accurate binding energies. Estimated CCSD(T)/aug-cc-pVTZ values were obtained by adding a ΔCCSD(T) correction, Equation (23), to MP2/aug-cc-pVTZ values.

$$\Delta CCSD(T) = E_{CCSD(T)}^{aug-cc-pVDZ} - E_{MP2}^{aug-cc-pVDZ} \tag{23}$$

We found this additive scheme effective in previous work.[119]

In addition to MP2 and CCSD(T), the spin component scaled MP2 (SCS-MP2)[44] method was explored. The SCS-MP2 method scales the MP2 parallel-spin and antiparallel-spin correlation energies with different scaling factors to obtain more accurate energies at the same computational cost as standard MP2. We used the scaling factors of Grimme (SCS-MP2)[44] and also those of Hill and Platts (SCSN-MP2).[49] The SC-MP2 scaling factors are 6/5 and 1/3 for the same spin and opposite spin correlation energies, respectively. The SCSN-MP2 scales the opposite spin correlation energy by 1.76 and does not include the same spin correlation in the total correlation energy (i.e., a scaling factor equal to 0). Density fitting (DF)[4,141] was used in all SCS and SCSN calculations. Density fitting greatly speeds up the computation with very little loss of accuracy in binding energies.

Second-order symmetry-adapted perturbation theory (SAPT2)[55,143] was used to obtain components of the interaction energy, such as electrostatic, dispersion, induction and exchange energies. The SAPT2002[13] and SAPT2006[12] packages were used in the present study. All SAPT2 results were computed with the aug-cc-pVDZ′ basis. SAPT divides the Hamiltonian (H) into a Fock Operator (F), an intermolecular operator (V), and an intramonomer operator (W),

$$H = F + V + W. \tag{24}$$

The SAPT interaction energy is divided into interactions at the Hartree-Fock level (E_{int}^{HF}) and the correlated component of the interaction energy (E_{int}^{CORR}),

$$E_{int}^{SAPT} = E_{int}^{HF} + E_{int}^{CORR}. \tag{25}$$

These components of the interaction energy can be further decomposed into various electrostatic (elst), exchange (exch), induction (ind) and dispersion (disp) energies, as shown in Equations (26) and (27).

$$E_{int}^{HF} = E_{elst}^{(10)} + E_{exch}^{(10)} + E_{ind,resp}^{(20)} + E_{exch-ind,resp}^{(20)} + \delta E_{int,resp}^{HF} \tag{26}$$

$$E_{int}^{CORR} = E_{elst,resp}^{(12)} + E_{exch}^{(11)} + E_{exch}^{(12)} + {}^{t}E_{ind}^{(22)} + {}^{t}E_{exch-ind}^{22} + E_{disp}^{(20)} + E_{exch-disp}^{(20)} \tag{27}$$

The superscript (ab) represents the order of the perturbation for operators V and W respectively. The components of the interaction energy may be collected as

$$E_{elst} = E_{elst}^{(10)} + E_{elst,resp}^{(12)}, \tag{28}$$

$$E_{exch} = E_{exch}^{(10)} + E_{exch}^{(11)} + E_{exch}^{(12)}, \tag{29}$$

$$E_{ind} = E_{ind,resp}^{(20)} + E_{exch-ind,resp}^{(20)} + \delta E_{int,resp}^{HF} + {}^{t}E_{ind}^{(22)} + {}^{t}E_{exch-ind}^{22}, \tag{30}$$

$$E_{disp} = E_{disp}^{(20)} + E_{exch-disp}^{(20)}. \tag{31}$$

For present purposes we have decided to classify the cross terms exchange-induction and exchange-dispersion as induction and dispersion, respectively.[120]

Potential energy surfaces (PES) were studied for four complexes in parallel-displaced orientations: benzene dimer, fluorobenzene-benzene, benzonitrile-benzene and phenol-benzene. The monomer geometries were obtained from MP2/aug-cc-pVDZ geometry optimization with the QCHEM package[61] and held at this rigid geometry in further calculations of the complexes. Potential energy surfaces of four complexes were scanned over three geometric parameters: the vertical interplanar distance (R1), the parallel displacement over a vertex (R2), and the parallel edgewise displacement (R3), as shown in Figure 1. All single point energy calculations were performed with the

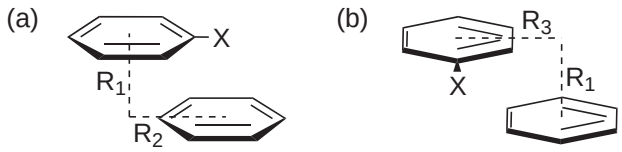

Figure 1: Substituted benzene-benzene complexes in (a) parallel-displaced over a vertex and (b) parallel-displaced edgewise orientations. X = H, F, CN, and OH

MOLPRO package.[140] All binding energies reported are corrected for basis set superposition error using the counterpoise method of Boys and Bernardi.[11] Core orbitals were constrained to be doubly occupied in all correlated computations.

2.2 Results and Discussion

Various levels of theory have been explored to determine a good balance between computational cost and accuracy. After justifying the use of the SCS-MP2/ATZ level of theory, more complete potential energy surfaces will be analyzed to determine how substituents and geometry affect the interaction energies of substituted benzene dimers in parallel-displaced configurations. Finally, SAPT analyses of selected orientations are used to elucidate the physical nature of the substituent effect by determining the components of the interaction energy.

The vertical displacement (R1), parallel displacement over a vertex (R2), and parallel displacement edgewise (R3) were systematically varied to sample different possible configurations (see Figure 1). The vertical displacement (R1) is defined as the distance from the center of the benzene ring to the plane of the ring below. An R2 or R3 displacement of 0.0 Å corresponds to the sandwich configuration, in which the geometric centers of the two rings are on top of one another. For the benzene dimer, the PES is symmetric about zero for R2 and R3. For the substituted complexes, negative R2 displacements move the substituent away from the other ring, and positive R2 displacements move the substituent over the other ring. Fluorobenzene-benzene and benzonitrile-benzene are symmetric about zero for edgewise displacements (R3).

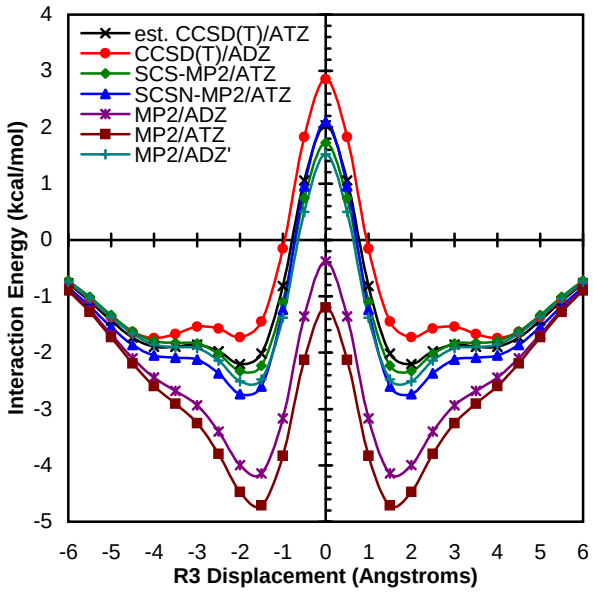

Figure 2: Interaction energy of benzene dimer parallel-displaced edgewise for various levels of theory. R1=3.3 Å.

However, this is not the case for phenol-benzene; negative R3 displacements point the hydrogen atom on the rigid hydroxyl group away from the benzene ring, and positive R3 displacements point this atom toward the benzene ring.

Figure 2 shows the performance of a variety of levels of theory for benzene dimer parallel-displaced edgewise. The estimated CCSD(T)/ATZ results are the most reliable of those considered here. CCSD(T)/ADZ underestimates the total interaction energy due to basis set incompleteness. The MP2/ADZ and MP2/ATZ levels of theory always overbind the dimer due to an incomplete description of electron correlation. The MP2/ADZ′ approach provides reasonably accurate results compared to the estimated CCSD(T)/ATZ benchmarks due to fortuitous cancellations of error from basis set incompleteness and an incomplete description of electron correlation. The SCS-MP2 and SCSN-MP2 methods perform well across the potential energy surface. SCSN-MP2 performs better around R2 values of zero, whereas SCS-MP2 performs better on average across the PES. It is interesting to note that MP2 with

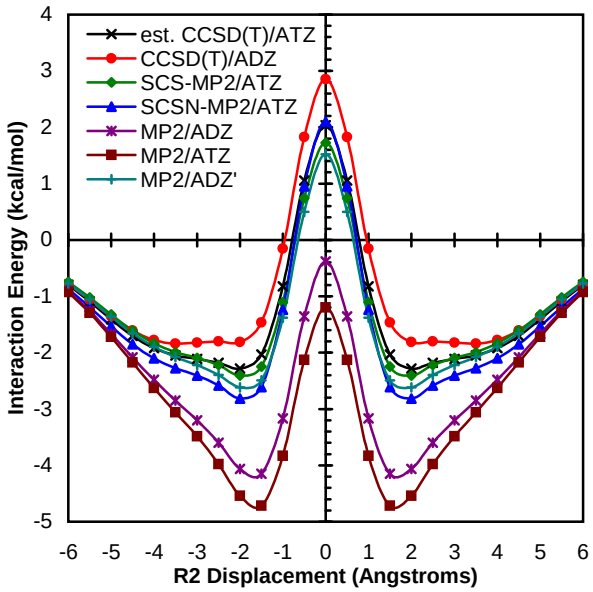

Figure 3: Interaction energy of benzene dimer displaced over a vertex for various levels of theory. R1=3.3 Å.

the truncated ADZ′ basis set does better than SCSN-MP2 on average. The maximum deviation for the SCS-MP2 method is smaller than the maximum deviation for SCSN-MP2. The maximum deviations occur at the sandwich configuration for SCS-MP2 and at the local minimum of the PES for SCSN-MP2.

In addition to the edgewise displacements it is important to determine how each method performs for parallel displacements over a vertex. As anticipated the methods behave similarly for benzene dimer parallel-displaced over a vertex, shown in Figure 3. SCSN-MP2 matches the estimated CCSD(T)/ATZ level of theory better than SCS-MP2 near the sandwich configuration. However, SCS-MP2 matches the curve better on average and has a smaller maximum deviation.

The SCS-MP2 method performs well for the substituted complexes fluorobenzene-benzene and benzonitrile-benzene, as shown in Figures 4 and 5 respectively. The MP2/ADZ and MP2/ATZ levels of theory overbind the substituted complexes; however, they have been removed from the figures to allow closer examination of the

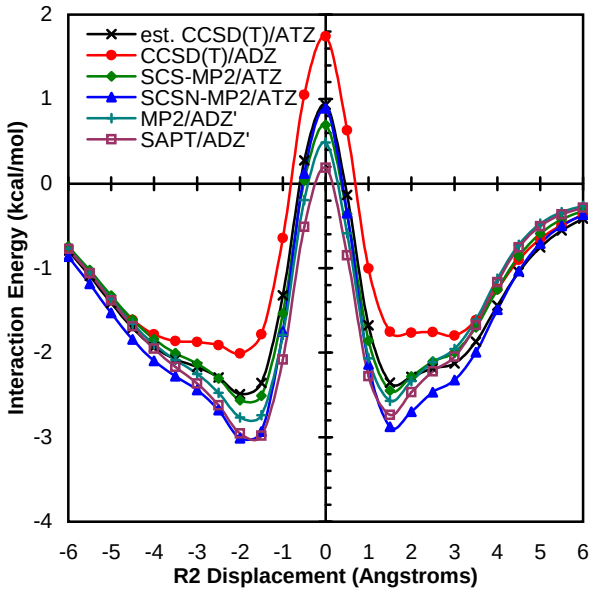

Figure 4: Interaction energy of fluorobenzene-benzene displaced over a vertex at various levels of theory. R1=3.3 Å.

other curves. For fluorobenzene-benzene, the SCSN-MP2 method performs better than SCS-MP2 near the sandwich configuration; however, on average SCS-MP2 outperforms SCSN-MP2. For benzonitrile-benzene, SCS-MP2 is closer to the estimated CCSD(T)/ATZ curve than SCSN-MP2 at all values of R2 except for R2=5.0 Å; however, at this point the two methods differ by less than 0.01 kcal mol^{-1}. Also in figures 4 and 5, SAPT2/ADZ′ is shown in comparison to the other levels of theory studied. SAPT/ADZ′ does a good job of staying parallel to the estimated CCSD(T)/ATZ curves, but it overbinds by several tenths of a kcal mol^{-1} for small R2 displacements.

Due to the high computational cost, estimated CCSD(T)/ATZ PES's were not computed for phenol-benzene or for benzonitrile-benzene and fluorobenzene-benzene in parallel-displaced edgewise orientations. However, SCS-MP2/ATZ PES's are always within 0.35 kcal/mol of the estimated CCSD(T)/ATZ potential energy surface for the systems where it was computed, strongly suggesting that this level of theory is appropriate for the other systems which are similar.

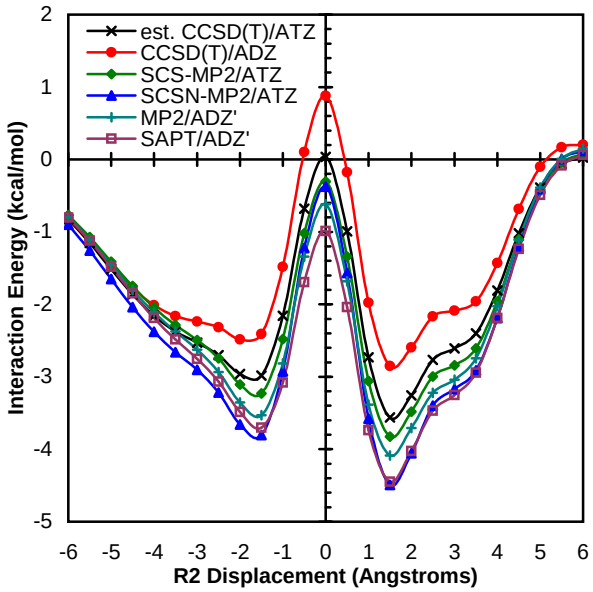

Figure 5: Interaction energy of benzonitrile-benzene displaced over a vertex at various levels of theory. R1=3.3 Å.

Figures 6 and 7 present SCS-MP2/ATZ results for parallel displacements over a vertex and over an edge, respectively. Optimal displacement sizes and interaction energies for our constrained potential surface scans are presented in Table 1. As indicated by the table, a single substituent can strengthen the binding by several tenths of a kcal mol^{-1} up to 1.5 kcal mol^{-1} in the case of benzonitrile-benzene. However, even though the potential surfaces are fairly flat, all of the substituted heterodimers have similar equilibrium geometries, with identical vertical displacements and horizontal displacements differing by no more than 0.2 Å from those in the parent benzene dimer.

In Figure 6 the substituent effect for the parallel-displaced over a vertex orientation is studied at three vertical separations. As previously observed,[118,120] all substituted complexes bind better than benzene dimer in the sandwich configuration. At a vertical

Table 1: Interaction energies (in kcal mol^{-1}) for the C_6H_6-C_6H_5X complexes at the SCS-MP2/aug-cc-pVTZ level of theory.[a]

Displaced Over a Vertex			
X	R1	R2	ΔE
H	3.5	1.7	-2.7
F	3.5	-1.6	-3.0
CN	3.5	1.5	-4.2
OH	3.5	1.5	-3.0
Displaced Edgewise			
X	R1	R3	ΔE
H	3.5	1.7	-2.7
F	3.5	1.6	-3.2
CN	3.5	1.5	-4.0
OH	3.5	1.6	-3.2

[a]Optimal displacements for constrained potential energy surface scans using parallel, rigid monomers with energies evaluated every 0.1 Å.

displacement of 3.3 Å (Figure 6a), fluorobenzene-benzene, phenol-benzene and benzene dimer have very similar binding energies for negative R2 displacements. Specifically, fluorobenzene-benzene binds slightly stronger than benzene dimer at all negative R2 displacements except those beyond -5.5 Å. Phenol-benzene binds more strongly than benzene dimer at small negative displacements, but binds slightly weaker than benzene dimer for R2 displacements between -2 and -5.5 Å. Benzonitrile-benzene always binds more strongly than benzene dimer except for positive displacements greater than 4.0 Å. For positive displacements of R2 (where the substituent crosses above the other ring), substituents cause stronger binding than in benzene dimer until a certain point along the potential energy surface. For fluorobenzene-benzene, this occurs early at 1.5 Å. For phenol-benzene and benzonitrile-benzene, this occurs at 4.0 Å. The origin of this behavior will be examined below using SAPT. However, we note that at shorter displacements, phenol-benzene and benzonitrile-benzene show a marked preference for having the substituent cross over the other ring (positive displacements) rather than to move away from it (negative displacements). This

preference can be as large as several tenths of one kcal mol^{-1} in some cases. On the other hand, except at very short displacements, in fluorobenzene-benzene the fluorine prefers to move away from the other ring rather than over it.

As the vertical displacement increases from 3.3 Å (Figure 6a) to 3.5 Å (Figure 6b), a few areas of the potential energy surface show significant change. For one, the interaction energy at the sandwich configuration decreases. This is not surprising, as the significant steric repulsion in the sandwich configuration will decrease significantly at the larger intermonomer distance. Next, the binding energies at the local minima decrease very slightly. However, the general trends of the substituent effect relative to benzene dimer stay consistent. In Figure 6c the vertical displacement is increased further to 3.7 Å. At this vertical displacement, the interaction energy at the sandwich configuration decreases further, but the general effect of the substituent stays consistent.

In Figure 7 the substituent effect for the parallel-displaced edgewise orientation is studied at three vertical separations. In general, the substituent does not dramatically affect the shape of the curve, except to enhance the binding relative to benzene dimer. Benzonitrile-benzene always binds more strongly than any of the complexes studied. Fluorobenzene-benzene and phenol-benzene bind more strongly than benzene dimer and have approximately the same interaction energy. All of the curves are symmetric about R3=0.0 Å except for phenol-benzene. For phenol-benzene the complex prefers positive R3 displacements where the hydrogen atom on the hydroxyl group points in the direction of the benzene molecule.

In order to gain more insight into the nature of the substituent effect in the complexes studied, we used SAPT to evaluate the electrostatic, dispersion, induction and exchange-repulsion components of the interaction energy across the entire potential energy curves for the configurations displaced over a vertex (Figure 1a). Due to their decreased symmetry (and concomitant increased computational costs), the

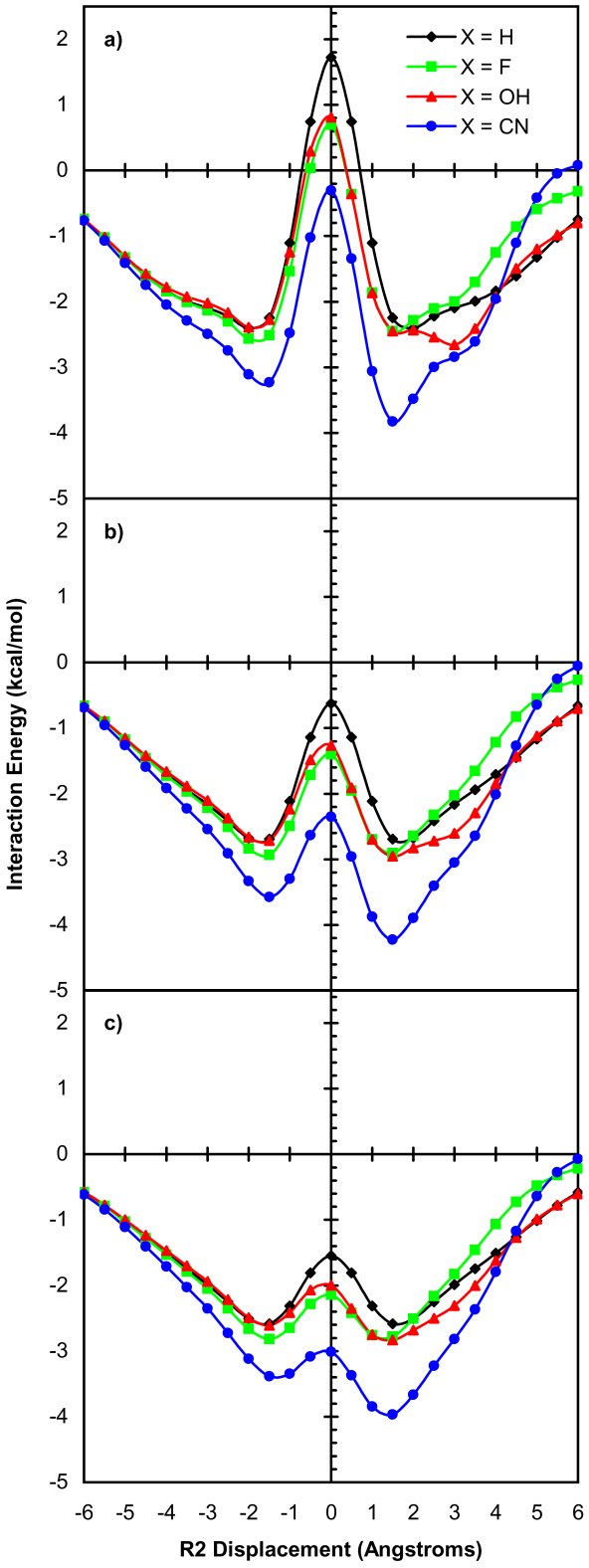

Figure 6: Comparison of substituents displaced over a vertex with SCS-MP2/ATZ. a) R1=3.3 b) R1=3.5 c) R1=3.7 Å.

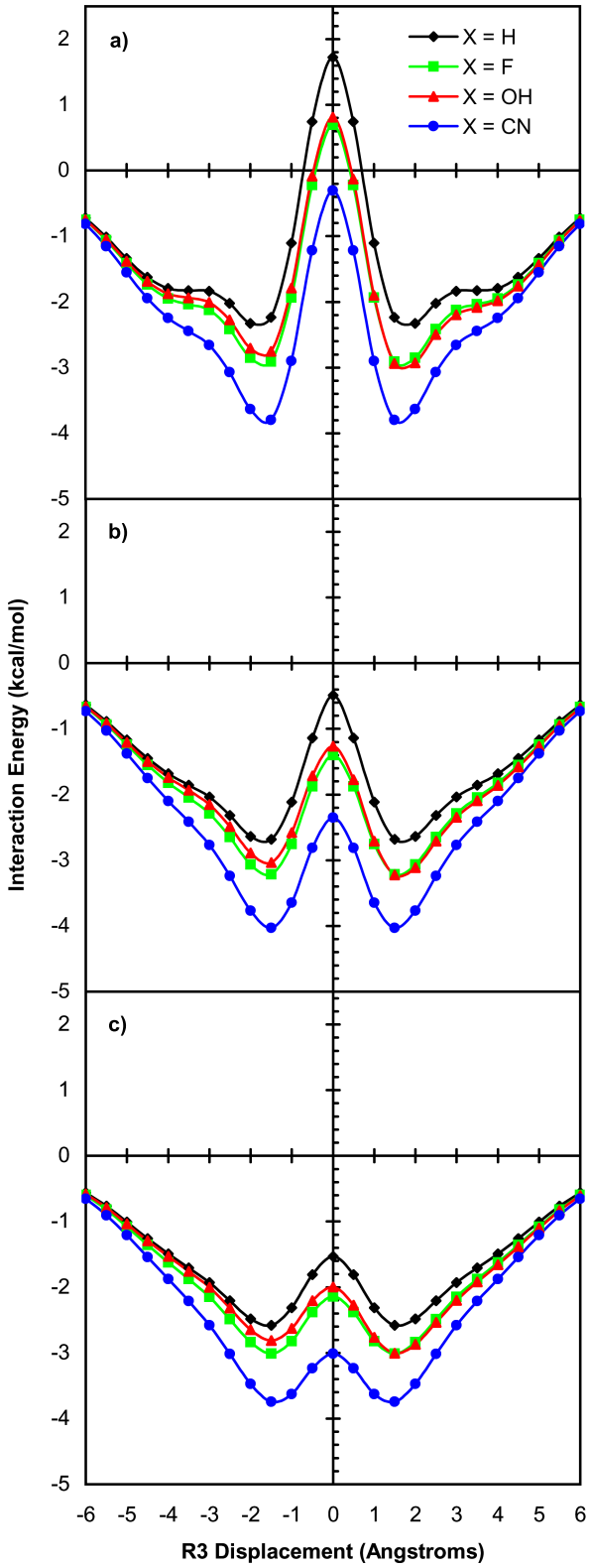

Figure 7: Comparison of substituents displaced edgewise with SCS-MP2/ATZ. a) R1=3.3 b) R1=3.5 c) R1=3.7 Å.

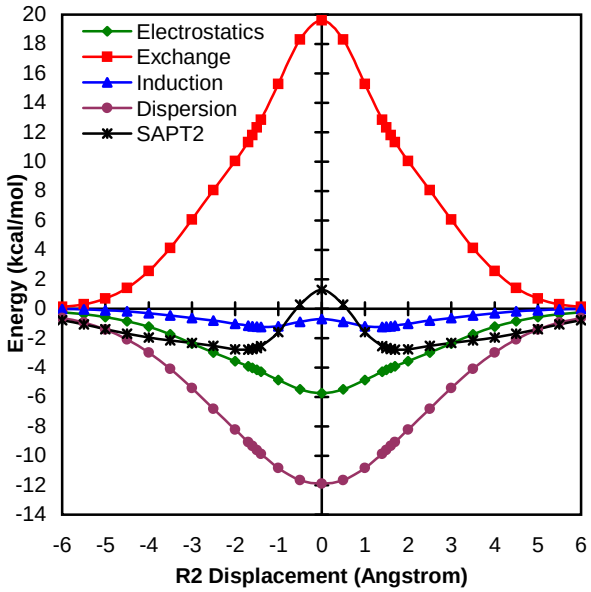

Figure 8: Components of the SAPT2 interaction energy for benzene dimer parallel-displaced over a vertex. R1=3.3 Å.

SAPT curves were not generated for the displaced edgewise complexes (Figure 1b). However, the binding of the displaced edgewise complexes is easier to explain, because the energy is dominated by ring-ring interactions that can be understood from computations at the sandwich configuration.

The components of the SAPT interaction energy are shown for the benzene dimer as a function of the displacement over a vertex in Figure 8. At the sandwich configuration (R2=0) exchange repulsion is at a maximum, whereas dispersion and electrostatics are at a minimum. The magnitude of the dispersion interaction is at a maximum at the sandwich configuration because the two monomers are the closest in this position. As the R2 displacement increases, the dispersive interactions become less attractive because the molecules are moving farther apart. Conversely, the exchange-repulsion component of the interaction energy is at maximum for the sandwich configuration because it has the greatest overlap between electron densities

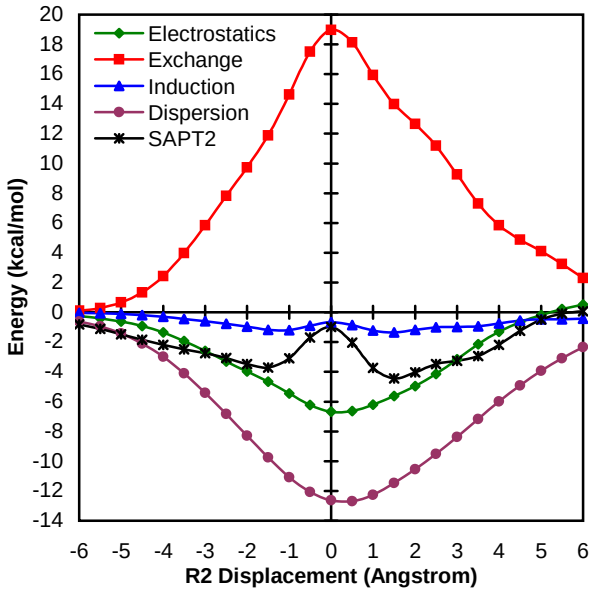

Figure 9: Components of the SAPT2 interaction energy for benzonitrile-benzene parallel-displaced over a vertex. R1=3.3 Å.

of the monomers. As the molecules move away from each other, the charge density overlap is reduced and the exchange-repulsion decreases. In general, induction does not contribute substantially to the total interaction energy; however, it is of interest to note that the induction is slightly less favorable at the sandwich configuration and obtains a local minimum near the local minimum of the total energy. The electrostatic component of the interaction energy is a minimum at the sandwich configuration. This may be something of a surprise if one considers that this configuration has the greatest overlap between the negative π clouds and places partially positive hydrogen atoms directly on top of each other. However, the π electron clouds interpenetrate and thus create an overall attractive electrostatic force. As the two molecules move apart, their electrostatic interaction decreases. The total interaction energy for benzene dimer as a function of the displacement over a vertex is determined by dispersion, exchange and electrostatics. A parallel-displaced configuration is preferred over the sandwich configuration because the electrostatic and dispersion

terms remain favorable for moderate horizontal displacements while the unfavorable exchange repulsion term decreases rapidly in magnitude.

The other complexes studied with SAPT have very similar trends in their components of the interaction energy. The most notable differences are observed for positive R2 displacements where direct substituent-π interactions are found. One example is shown for benzonitrile-benzene in Figure 9. This example is shown because it deviates to the largest extent from benzene dimer. It is interesting to note that the shape of the curve looks very similar to benzene dimer for negative R2 displacements. In order to determine the direct substituent effect, the components of the benzonitrile-benzene interaction energy relative to benzene dimer are shown in Figure 10b.

For Figure 10 we will first focus on the positive R2 displacements where direct substituent-ring interactions are found. The components of the interaction energy of fluorobenzene-benzene relative to benzene dimer are shown in Figure 10a. In general the induction and dispersion interactions are approximately the same in fluorobenzene-benzene and benzene dimer. One might have expected the dispersion interaction to be larger in fluorobenzene-benzene (due to the larger number of electrons on fluorine versus hydrogen), but apparently the very electronegative nature of fluorine keeps it from being very polarizable. The exchange repulsion and electrostatic terms dominate the relative interaction energy. There is a dip in the relative exchange-repulsion term around R2 = 3 Å, when the fluorine is approximately above the middle of the other ring. For very small positive displacements R2, the electrostatic term is more favorable for fluorobenzene-benzene than for the benzene dimer primarily for two reasons. First, there is a favorable electrostatic interaction between the partial-negative fluorine atom and the partial-positive hydrogen from the other ring below it. Second, the ring-ring interaction is more favorable because fluorine has reduced the amount of negative π density in the ring, so there is less negative charge

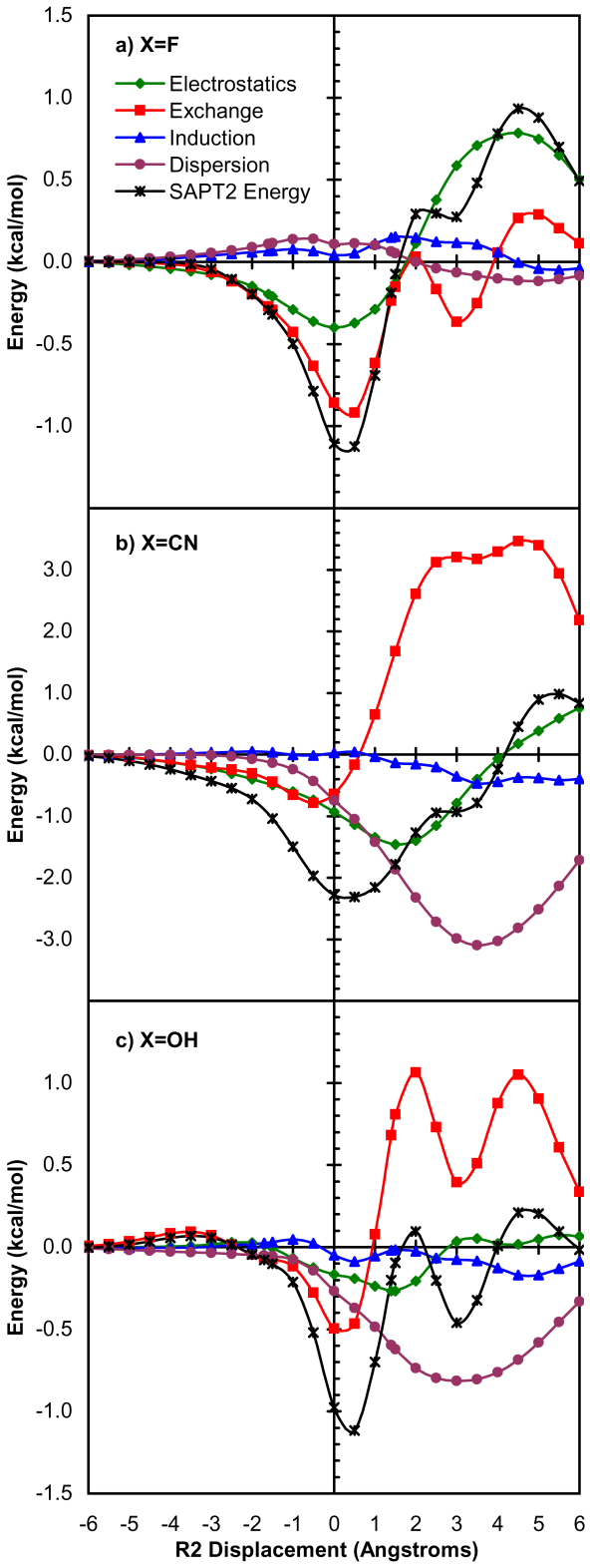

Figure 10: Components of the SAPT2 interaction energy relative to benzene dimer for a) fluorobenzene-benzene, b) benzonitrile-benzene, and c) phenol-benzene parallel-displaced over a vertex. R1=3.3 Å.

to interact with the negatively charged π ring of benzene below.[118,120] As the substituent starts to cross above the benzene ring below it, the electrostatic interaction becomes unfavorable relative to benzene dimer. This is mainly due to the repulsive interaction between the negative substituent and the π cloud. Once the aromatic rings are no longer overlapping (around displacements of 6 Å and larger), one might suppose the electrostatic term would become more favorable than that in the benzene dimer because of favorable interactions between a partial-negative fluorine on fluorobenzene and a partial-positive hydrogen on benzene. However, although these atoms are the ones in closest contact, the next-nearest atoms cannot be ignored. The C–F and C–H bonds in closest contact form bond dipoles which interact unfavorably because they point in the same direction.

The benzonitrile-benzene complex binds more strongly than benzene dimer for all R2 displacements less than 4.0 Å, as shown in Figure 10b. At the sandwich configuration, the electrostatic and dispersive forces are more attractive in benzonitrile-benzene than benzene dimer. The larger dispersion interaction is not surprising given that the nitrile group will be more polarizable than a hydrogen atom. The nitrile group is also strongly electron-withdrawing, leading to a reduced negative charge for the π-cloud.[118,120] This also leads to reduced steric repulsion between the two π-clouds, as evidenced by a less repulsive exchange term. As the nitrile group is moved across the face of the other ring (positive R2 displacements), the direct substituent-ring interaction has a very significant effect and large differences are observed in the components of the interaction energy relative to benzene dimer. The only exception is the induction component which is only slightly more attractive in benzonitrile-benzene than in benzene dimer. One would expect the induction term in benzonitrile-benzene to be more favorable than in benzene dimer because benzonitrile has a permanent electric dipole moment; the only surprise is perhaps how little this improves the induction term. As the nitrile substituent displaces across the other ring, dispersive interactions

become much more favorable because nitrile is larger and more polarizable than the hydrogen it replaces in the parent benzene dimer. On the other hand, the exchange interaction becomes more repulsive.

The electrostatic interaction remains more favorable than in benzene dimer for modest displacements R2, with the most improvement occurring near R2 = 1.5 Å. At this point, the partially positive carbon of the nitrile substituent is vertically aligned with a partially negative carbon of benzene, and the partially negative nitrogen is aligned with a partially positive hydrogen of benzene, leading to an enhancement of about 1.5 kcal mol^{-1} for the electrostatic attraction. As one continues toward larger displacements R2, this improvement in the electrostatic interaction compared to benzene dimer becomes smaller. At large displacements, the electrostatic interaction becomes less favorable than benzene dimer (just as for fluorobenzene-benzene) because the nitrile C–N and benzene C–H bond dipoles are aligned in the same direction.

The SAPT interaction energies for phenol-benzene are shown relative to benzene dimer in Figure 10c). At the sandwich configuration, all of the components of the interaction energy are more favorable than in benzene dimer. For positive R2 displacements, dispersion and exchange have a large effect on the relative binding energies. The exchange-repulsion term is less favorable for phenol-benzene compared to benzene dimer, primarily due to greater steric repulsion with the π-cloud below for hydroxyl than for a hydrogen. There is a dip in the relative exchange contribution around 3 Å, when the hydroxyl is above the middle of the other ring. The large difference in the dispersion term between phenol-benzene and benzene dimer is attributed to both a larger number of electrons and a more polarizable hydroxyl group in phenol-benzene. Dispersion is not as important for the relative binding of phenol-benzene as it is for benzonitrile-benzene, but it is much more important than in fluorobenzene-benzene; overall, dispersion can favor phenol-benzene over benzene

dimer by several tenths of one kcal mol^{-1}. Electrostatically, even though hydroxyl is a strongly electron donating substituent in contexts like electrophilic aromatic substitution reactions, it has remarkably little effect on the π-cloud density of an unreacting phenyl ring.[118,120] Consistent with this observation, the electrostatic contribution in phenol-benzene is rather similar to that in the benzene dimer near the sandwich configuration. It remains similar for larger positive displacements R2, perhaps because direct ring-substituent interactions may be rather similar in size but opposite in magnitude for the partial-positive hydrogen and the partial-negative oxygen of the hydroxyl group.

In contrast to the positive displacements over a vertex, negative displacements have a smaller effect on the components of the interaction energy and are similar for the different substituents. For negative displacements the interaction energy is predominantly determined by ring-ring interactions and the effect of the substituent on the electronic structure of the ring (as opposed to direct ring-substituent interactions as found in positive R2 displacements). For negative R2 displacements of fluorobenzene-benzene (Figure 10a), the induction and dispersion energies are slightly less favorable (by about 0.1 kcal mol^{-1} or less) than in the benzene dimer. The electron-withdrawing fluorine atom decreases the electron density of the ring of fluorobenzene and the very electronegative nature of the fluorine atom cause it to hold tightly to the extra electrons in the system, leading to a less favorable dispersive energy as compared to benzene dimer. At negative displacements, fluorobenzene-benzene is more favorable electrostatically than benzene dimer because the electron-withdrawing fluorine causes the fluorobenzene ring to be slightly more positive electrostatically and increases the electrostatic ring-ring attraction. Additionally, the reduced π-electron density in fluorobenzene leads to a substantially reduced exchange-repulsion interaction between the two molecules.

For negative R2 displacements of benzonitrile-benzene, the dispersion, electrostatic, and exchange-repulsion are all more favorable than benzene dimer (Figure 10b). Just as in fluorobenzene-benzene, although to a greater degree, the electron-withdrawing substituent causes the π-cloud in benzonitrile to be less negative than the π-cloud of benzene.[118,120] This leads to an enhanced electrostatic attraction in the complex at negative displacements. In addition, the substituent removes electron density from the ring causing the exchange component to be less repulsive in benzonitrile-benzene than benzene dimer. The dispersion is slightly larger in benzonitrile-benzene because of the larger number of electrons participating in the interaction. This dispersive attraction decreases as the substituent moves away from the benzene ring and becomes nearly identical to benzene dimer for displacements less than -2.0 Å.

For negative displacements of phenol-benzene, the relative components of the interaction energy are very similar to benzene dimer (Figure 10c). The total energy of phenol-benzene relative to benzene dimer is predominantly controlled by the exchange-repulsion. At small negative displacements, the electrostatic and dispersion energies are slightly more favorable.

Finally, the substituent effects for edgewise displacements, shown in Figure 7, are very similar to the displacements over a vertex when the substituent is pulled away from the other ring (negative R2 values in Figure 1a). The effect of the substituent is felt primarily through its influence on the electronic structure of the ring to which it is bonded, leading to modified ring-ring interactions just as in the negative R2 over-vertex displacements just discussed. Comparing the edgewise displacements in Figure 7 to the negative R2 over-vertex displacements in Figure 6, the edgewise displacements are somewhat more favorable, particularly for benzene-benzonitrile.

2.3 Conclusions

The effect of substituents on parallel-displaced π-π interactions has been explored as a function of vertical and horizontal displacements of the rings. The present results have allowed for a deeper understanding of both direct substituent-ring interactions and the effect of the substituent on the π-π interaction in a variety of geometries. Substituents have a complicated effect on the potential energy surface that can be favorable or unfavorable. At short horizontal displacements, substituents tend to enhance π-π interactions through a mixture of electrostatic, dispersion, and exchange-repulsion terms, as discussed in previous work on sandwich dimers.[120,121] However, at larger horizontal displacements over a vertex, direct interactions between the substituent and the ring below it can diminish the interaction energy, particularly for substituents like fluorine with significant partial negative charges. Strongly polarizable substituents, such as hydroxyl, can lead to overall favorable substituent-ring interactions, in this case mainly due to enhancement of the dispersion interaction. At large horizontal displacements over a vertex, the biggest net effect relative to benzene dimer seems to be the electrostatic interaction between the bond dipoles of the closest interacting bonds, i.e., the C–H bond of benzene and the nearest bond of the substituent. This interaction is unfavorable for fluorine and nitrile substituents.

CHAPTER III

BENCHMARK FULL CONFIGURATION INTERACTION AND EOM-IP-CCSD RESULTS FOR PROTOTYPICAL CHARGE TRANSFER SYSTEMS: NONCOVALENT IONIZED DIMERS

Ionized noncovalent dimers are relevant in electron/hole transfer (E/HT) processes ubiquitous in biophysics and molecular electronics,[5,39,42,86] and are described by open-shell doublet wave functions. Solvents used in radioactive element separation are susceptible to radiation induced ionization, which in the case of neat aromatic liquids leads to the initial formation of aromatic cations and dimer cations like $(C_6H_6)_2^+$ and $(C_5H_5N)_2^+$.[40,52,90] Knowledge of the cation potential energy surface (PES) is needed in the interpretation of photoelectron spectra of neutral dimer species.[1,45,63] $(O_2)_2^+$ is an intermediate in the formation of protonated water clusters in the lower ionosphere.[41,73,100] Cation dimers of polyaromatic hydrocarbons are suspected to be the source of broad extended interstellar emission.[101] However, even in the case of simple isolated systems, like $(O_2)_2^+$, $(CO_2)_2^+$, $(C_6H_6)_2^+$ and $(H_2O)_2^+$, the structure and properties have long eluded both theorists and experimentalists alike.[30,48,51,89,114,126]

For condensed phase problems Marcus theory[78–80] provides the relationship between the kinetics of the E/HT transfer processes and the electronic coupling between localized donor and acceptor sites. Often donor or acceptor sites are made up of dimer or multimeric cores, for example the special pair of bacteriochlorophylls which serves as the electron donor in the photosynthetic reaction center.[88,147] In cytochrome *c* of bacterium *Schewanellaoneidensis* MR-1 several heme groups acting concertedly are implicated in the reduction process, and, consequently, make the ET process more

efficient. This efficiency, referred to as 'electron harvesting', has been attributed to the closely packed arrangement of the heme groups.[72,125] Oxidative damage on DNA leads to facile hole transfer between stacked aromatic bases.[32]

To explain and understand the function of these important biological systems, as well as to engineer new compounds, one must obtain knowledge of the energetics and properties of the states involved. Especially vital is the value of the diabatic coupling between the donor and acceptor moieties, which should be calculated with an accuracy independent of relative orientations and distance between the two.

Several problems arise in approximate electronic structure calculations of doublet systems. Single reference approaches based on an open-shell doublet reference are plagued by symmetry breaking,[29,107] even when highly correlated wave functions are used. Typically, the initial and final states involved in the hole/electron transfer process are nearly degenerate, and the wave functions acquire a considerable multi-determinantal character. To this end multireference (MR) approaches have been used;[16,19,104] however, artificial symmetry breaking can occur for MR wave functions as well.[36] Moreover, it requires the choice of an active space and may lead to unbalanced description of electronic states along the CT path. Recently, the spin-flip (SF) approach[64,65,70] based on the quartet reference has been tested.[146] Although SF wave functions include all the leading electronic configurations, the quartet reference exhibits instability, which affects the quality of the PES.

The symmetry breaking problem is most readily manifested in the case of open-shell symmetric dimers, i.e., when the donor and acceptor moieties are indistinguishable. In this case, there are two Hartree-Fock (HF) solutions: the delocalized wave function, which has a correct symmetry, and a lower-energy symmetry-broken one. The energetic difference persists even at correlated levels of theory and vanishes only in the full configuration interaction (FCI) limit, where the correct symmetry is restored. For example, in the case of the ethylene dimer cation studied herein the

difference between the symmetric and symmetry-broken HF solutions is 0.2 eV. One thus faces a dilemma of which solution to choose.[74] The symmetric, charge delocalized solution has the correct symmetry at the symmetric nuclear configuration, but it may not be the best solution in a variational sense. On the other hand, the lower-energy solution does not exhibit the proper symmetry of the molecule at the symmetric nuclear configuration, and can therefore exhibit unphysical properties (such as artificially nonzero dipole moments). Moreover, from a practical point of view, the presence of these two different solutions can cause severe difficulties. Straightforward application of electronic structure programs will typically lead to the lower-energy, symmetry-broken solution being found at nonsymmetric geometries, and the higher-energy, symmetric solution being found at the symmetric geometry. This would lead to an undesirable and artificial discontinuity in the potential energy surface. Vibrational frequencies can be adversely affected no matter which solution is chosen.[23]

CT systems also pose challenges to density functional theory (DFT) due to self-interaction error (SIE), of which the H_2^+ dissociation curve is the most striking example.[7] SIE, which is present in many functionals, causes artificial stabilization of delocalized charge,[75,137,148] which spoils the description of Rydberg and CT excited states (see, for example, Refs.[34] and[35]), vibronic interactions,[124,138] and charge distribution in the ground-state CT systems.[75]

This work presents FCI calculations of PESs and properties and demonstrates how to alleviate the problems mentioned above using single-reference equation-of-motion coupled-cluster model for ionized systems (EOM-IP-CC) methodology. A suitable reference in this case is the neutral HF wave function, which does not suffer from the instability problems as all the electrons are paired. The ionic wave functions are derived by removing an electron. Implementation of this Koopmans-like idea within coupled-cluster (CC) framework is the essence of the EOM-IP-CC method.[20,92,116,117,129,130] This method has been applied earlier by Hsu to a series of alkyl compounds and

ethylene dimer, but no extensive testing was performed.[144] A similar approach, albeit based on the truncated configuration interaction (CI) method, has been developed by Simons for the calculation of ionization energies and electron affinities.[115] Similar ideas are exploited by related symmetry-adapted cluster CI family of methods.[84,85]

Here, EOM-IP-CCSD and FCI results for open-shell dimer cation species are compared. To the best of our knowledge there are no previous full CI benchmarks analyzing symmetry breaking in radical cations of van der Waals dimers. The evaluated quantities pertain to charge transfer states, i.e. charge localized on either fragment. We compute the absolute energy, permanent dipole, transition dipole and electronic coupling. The coupling is evaluated using the Generalized Mulliken-Hush[18,19] (GMH) model. Instead of the permanent dipole, which is origin-dependent for a charged system, we report the charge on the more positive molecule. This is also a measure of the weight of a particular diabatic (defined as a charge-localized state) state in the wave function:

$$q_A = \langle a\Psi_{A^+B} + b\Psi_{AB^+} | \hat{q_A} | a\Psi_{A^+B} + b\Psi_{AB^+} \rangle = |a|^2 \tag{32}$$

where q_A is the charge on fragment A and $\hat{q_A}$ is the associated operator.

The next section describes theoretical methods (EOM-CC approach to open-shell doublet wave functions and generalized Mulliken-Hush diabatization scheme) and computational details. Results for the selected benchmark systems are give in Section 3.2. The studied systems are: He_2^+, $(H_2)_2^+$, $(BH\text{-}H_2)^+$, $(Be\text{-}BH)^+$, and $(LiH)_2^+$. They were chosen based on the feasibility of FCI calculations and the difference of IEs. Finally, the EOM-IP-CCSD methodology is applied to the ethylene dimer, an often studied model system for polymer conduction and π interactions.[56,77,104,144,146] Our final remarks are given in Section 3.3.

3.1 Methodology

3.1.1 EOM-CC approach to open-shell and electronically excited species

The EOM approach[9,37,43,70,106,111,128] allows one to describe many multi-configurational wave functions within a single-reference formalism.[8] Conceptually, EOM is similar to CI: target EOM states are found by diagonalizing the so-called similarity transformed Hamiltonian $\bar{H} \equiv e^{-T} H e^{T}$:

$$\bar{H} R = E R, \tag{33}$$

where T and R are general excitation operators with respect to the reference determinant $|\Phi_0\rangle$. Operator T describes the dynamical correlation, while R allows one to access a variety of multideterminantal target states. Regardless of the choice of T, the spectrum of $\bar{H}$ is exactly the same as that of the original Hamiltonian H. Thus, in the limit of the complete many-electron basis set, EOM is identical to FCI. In a more practical case of a truncated basis, e.g., when T and R are truncated at single and double excitations, the EOM models are numerically superior to the corresponding CI models,[91] because correlation effects are "folded in" in the transformed Hamiltonian, while the computational scaling remains the same. Moreover, the truncated EOM models are rigorously size-consistent (or, more precisely, size intensive),[65,82] provided that the amplitudes T satisfy the CC equations for the reference state $|\Phi_0\rangle$ and are truncated at sufficiently high level of excitation consistent with that of R as follows:

$$\langle \Phi_\mu | \bar{H} | \Phi_0 \rangle, \tag{34}$$

where Φ_μ denotes μ-tuply excited determinants, e.g., $\{\Phi_i^a, \Phi_{ij}^{ab}\}$ in the case of CCSD.

By combining different types of excitation operators and references $|\Phi_0\rangle$, open-shell doublet states can be accessed in different ways, as explained in Figure 11. For example, we may use the open-shell doublet reference and operators R that conserve the number of electrons and a total spin.[60,111,128] In this case, one CT state will be described at the CC level, while the other one at the equation-of-motion

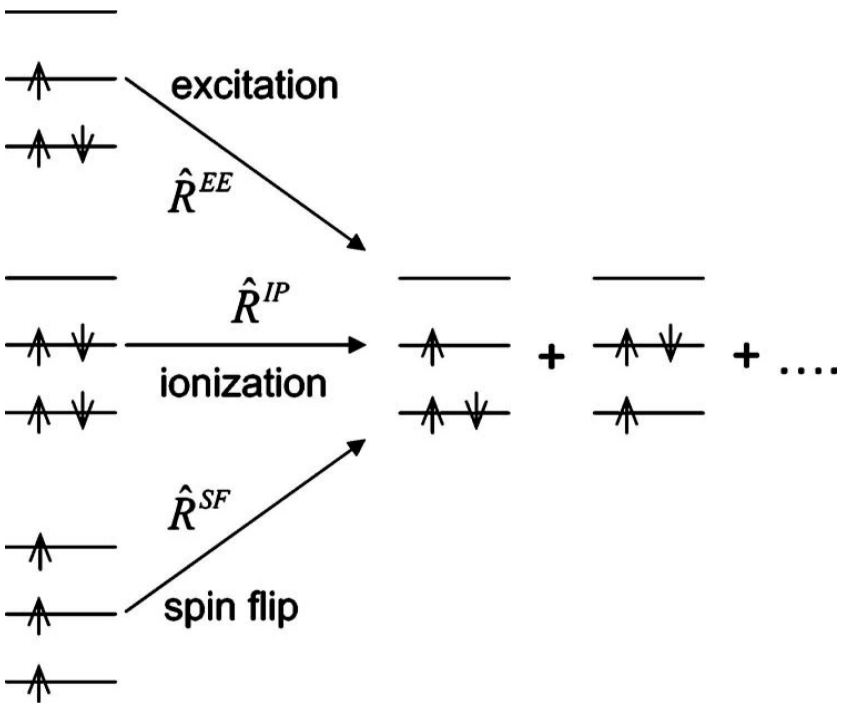

Figure 11: Open-shell doublet wave functions can be described by several EOM approaches using different references/excitation operators. The EOM-IP method employs a well-behaved closed-shell reference.

coupled-cluster for excitation energies (EOM-EE-CC) level. Problems arise due to the instability of the reference and unbalanced description of the two states. Inclusion of higher excitations, e.g., within EOM-CCSDT or EOM-CCSDt schemes[62,108] will of course improve the description, but at the price of increased computational costs.

The ionized/electron attached EOM models,[87,92,116,117,129,130] which employ operators R that are not electron conserving (i.e., include different number of creation and annihilation operators), describe ground and excited states of doublet radicals on equal footing. In our case, we start with a neutral reference and treat both CT states as ionized states. The truncation of EOM-IP operators deserves additional comments. For CCSD references, i.e., when operator T includes single and double excitations, the most common strategy is to retain only $1h$ and $2h1p$ operators as

follows:

$$R^{IP} = \sum r_i i + \sum r_{ij}^{a} a^{+} j i, \tag{35}$$

which gives rise to the EOM-IP-CCSD method. However, one may consider including $3h2p$ operators as well, as in EOM-IP-CC(2,3).[57,109] As demonstrated by Piecuch and Bartlett, this does not break the size consistency of the resulting EOM-IP method,[94] in contrast to EOM-EE,[123] thus justifying such a truncation scheme.

Finally, the EOM-SF method,[64,65,70] in which the excitation operators include spin-flip, allows one to access diradicals, triradicals, and bond-breaking without using spin- and symmetry-broken unrestricted HF (UHF) references. In our cases quartet reference would be used, as first proposed by You et al.[146] The obtained set of determinants is appropriate for the description of CT states, but the reference still exhibits instability.

To summarize, the EOM-IP method avoids the HF instability problems and describes problematic open-shell doublet states in a single reference formalism.

3.1.2 Generalized Mulliken-Hush model

Figure 12 presents the PESs along the CT reaction coordinate. The solid lines represent the adiabatic energies, i.e., the eigenvalues of the electronic Hamiltonian. The dotted lines are the diabatic energies. The corresponding wave functions depend only weakly on nuclear configuration and describe the charge-localized states, i.e., $A^{+}B$ and AB^{+}. The magnitude of the electronic coupling between these wave functions determines the kinetics of the process within Marcus theory. Note that electronic structure packages yield *adiabatic* energies and wave functions.

The transformation between the two basis sets is not straightforward because diabatic states are not rigorously defined in a general case.[81] We employed the GMH method developed by Robert Cave and Marshall Newton to compute the diabatic-adiabatic transformation matrix and the coupling elements. The method is based

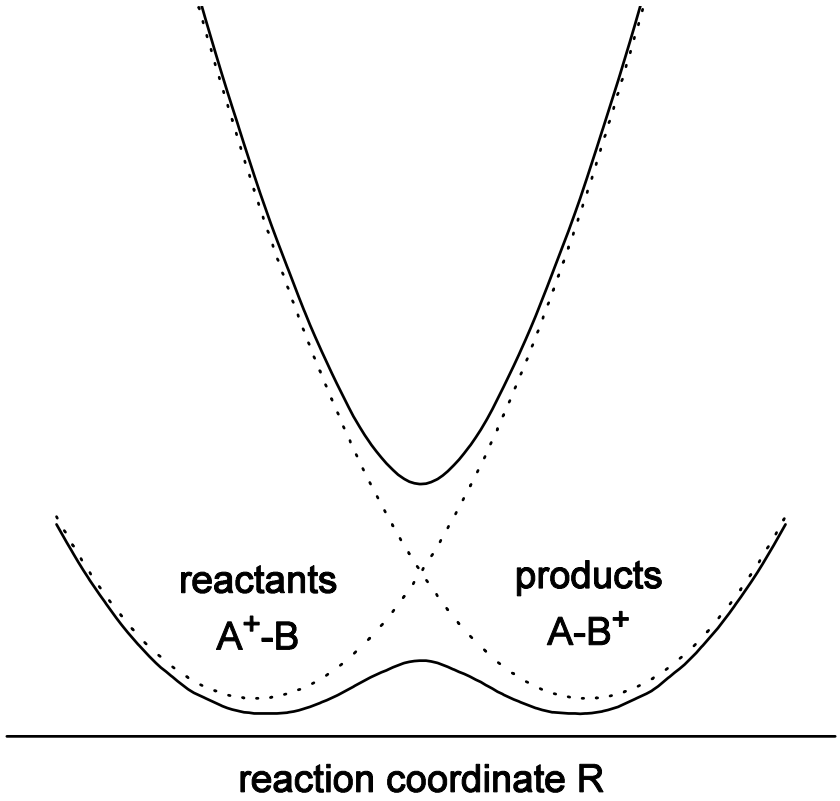

Figure 12: Diabatic (dashed line) and adiabatic potential energy surfaces for electron transfer reactions. Diabatic states correspond to reactant and product electronic wave functions, i.e. the charge fully localized on one of the species, while adiabatic states are eigenfunctions of the electronic Hamiltonian. Marcus theory relates the coupling between diabatic states to the rate of electron/hole transfer process.

on the assumption that there is no dipole moment coupling between the diabatic states, and thus the dipole moment matrix is diagonal in this representation. This corresponds to the two states with the largest charge separation, i.e. charge localized on the reactants and products. The so-defined transformation matrix can hence be applied to the Hamiltonian matrix in the adiabatic representation yielding the coupling as the off-diagonal element. This leads to the following expression:

$$h_{ab} = \frac{\mu_{12}\Delta E_{ab}}{\Delta\mu_{ab}} = \frac{\mu_{12}\Delta E_{12}}{[(\Delta\mu_{12})^2 + 4(\mu_{12})^2]^{1/2}} \tag{36}$$

The letter and number subscripts refer to diabatic and adiabatic quantities, respectively. μ_{12} is the transition dipole moment and $\Delta\mu_{12}$ is the difference between

the permanent dipole moments. Components of each vector in the direction defined by the permanent dipole difference vector for the initial and final adiabatic states are used. In the case of a charged system the definition of the dipole moment depends on the origin. However, the diagonalization matrix depends on the *difference* rather than the values itself and thus is origin independent.

The main forte of the GMH model is its simplicity and a wide range of applicability. It can be applied both to the ground state and excited state at any nuclear configuration. Furthermore, the only required quantities are adiabatic, and thus easily available using standard electronic structure software.

Similar diabatization schemes exploiting differences in molecular properties of the diabatic states have been explored in other applications as well.[3,15,33,76,142,145]

3.1.3 The CT reaction coordinates

The two important coordinates for CT processes are the intermolecular separation and the intramolecular CT coordinate described below. In the charge transfer processes (Figure 12) the reactants correspond to an electron/hole localized on one of the moieties, e.g. A^+-B. At infinite separation, the geometry of A is that of the cation, whereas the geometry of B is that of its neutral. The reaction corresponds to the positive charge moving from A to B and the nuclei rearranging such that A has the geometry of the neutral form and B has a cation-like geometry. At smaller interfragment separations, the geometries of the fragments along the reaction coordinate may differ from that simple picture. In principle, the geometries along this path can be calculated by following the energy minimum, i.e., conducting constrained optimization at each point along $A^+B \rightarrow AB^+$. Alternatively, a CT reaction coordinate can be approximated by arithmetic averaging of the Cartesian monomer coordinates:

$$\begin{aligned} Q_{R1} &= (1-R)\cdot Q_1 + R\cdot Q_2 \\ Q_{R2} &= R\cdot Q_1 + (1-R)\cdot Q_2 \end{aligned} \tag{37}$$

where Q_1 is the geometry of the neutral and Q_2 is the geometry of the cation. The averaging is done with the rotation axes and the centers of mass aligned. When R=0, A has its cation geometry, whereas B has its neutral geometry. At R=0.5 the geometry of each species is a simple average of the cation and neutral forms. Finally, at R=1 the geometry of A is that of the neutral, and that of B corresponds to the cation form. This approach merely ensures a smooth interpolation between the initial and final geometries and should not be taken as the path followed in a physical situation.

3.1.4 Computational details

Configuration-interaction singles (CIS), EOM-IP-CCSD (IP-CCSD/$2h1p$), EOM-IP-CC(2,3) (IP-CCSD/$3h2p$), and EOM-CCSD for excitation energies (EOM-EE-CCSD) calculations as well as all geometry optimizations were performed using the *QCHEM ab initio* package.[112] FCI calculations employed the PSI3 package.[28] Multireference configuration interaction (MRCI) calculations were performed using MOLPRO.[140] All basis sets were obtained from the EMSL repository.[38]

The charge localized on the monomers was computed assuming that charges on individual fragments are point charges located at the center of mass of individual fragments. Only the component of the total dipole moment in this direction is considered. Charge q_A is localized on fragment A at position r_A, while charge $(1 - q_a)$ is on fragment B localized at r_B. This yields the following expression for the charge:

$$q_A = \frac{-\mu + r_B}{r_B - r_A}, \tag{38}$$

where the dipole moment vector μ is defined to point towards the positive charge. Vector quantities are computed relative to the center of mass of the system.

Spin-restricted references were used in EOM-IP-CC and FCI calculations. EOM-EE-CCSD calculations were based on spin-unrestricted references for H_2 dimer. Otherwise, spin-restricted open-shell references (ROHF) were employed. For ethylene dimer, we considered both ROHF and UHF doublet references. CCSD energies were

converged to 10^{-10} hartree. Davidson iteration in EOM calculations were considered converged when the residue of the excited state vectors was below 10^{-10}. EOM-IP-CC(2,3) dipole moments for $(C_2H_4)_2^+$ were computed via finite differences using field values of ± 0.00001 a.u.

All electrons were active in EOM calculations. EOM dipole moments were calculated using fully relaxed one-particle density matrices, that is, including the amplitude and orbital response contributions,[71] while transition dipoles were computed as "expectation values", that is, using unrelaxed density matrices of the right-hand and left-hand eigenvectors.[128]

FCI properties were computed using unrelaxed density matrices. Orbital response terms are not needed in FCI property computations because the FCI properties are invariant to unitary transformations of the active orbitals; the exception occurs when some orbitals are frozen in the correlated computation, as was the case here for the $1s$-like orbitals for Be and B atoms. However, limited tests indicate that these core-active orbital rotations did not contribute significantly for the cases considered.

MRCI calculations employ the state-averaged complete active space self-consistent field (SA-CASSCF) reference and include all single and double excitations from the reference (MR-CISD).[139] To correct for the lack of size extensivity, the resulting MR-CISD energies are augmented by the Davidson correction[67] and are denoted as MR-CISD+Q. Unfortunately, no analog of the Davidson correction for properties is available. The active space consisted of the ethylene π and π^* orbitals. The SA-CASSCF computations include the ground state and the first excited state with equal weights. The four $1s$ carbon orbitals were restricted in CASSCF calculations and frozen in MR-CISD.

Geometries of H_2, BH, and LiH were optimized using CCSD(T) and the aug-cc-pVTV basis set. C_2H_4 and $C_2H_4^+$ structures were obtained using DFT with the B3LYP[10] functional and the 6-311+G* basis set.

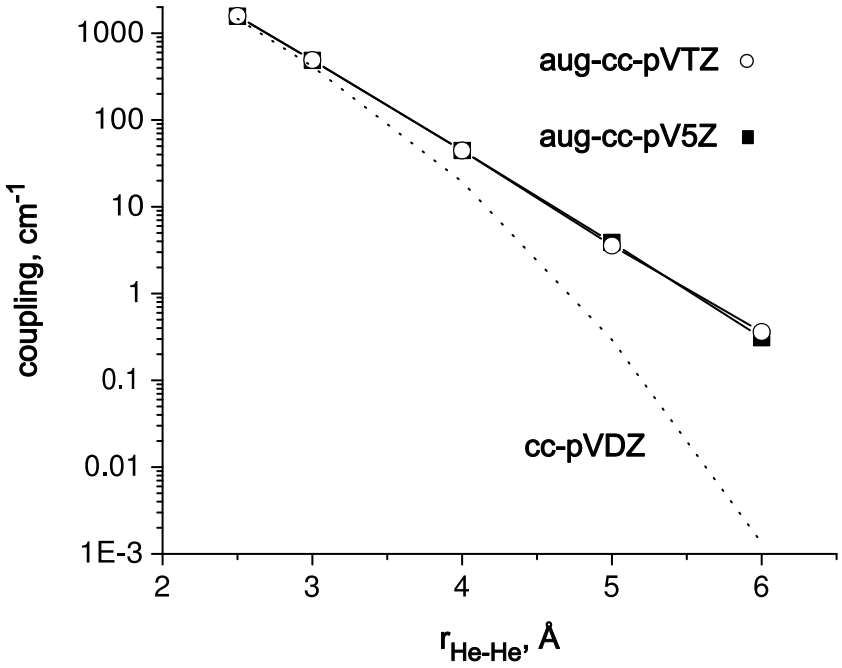

Figure 13: Electronic coupling in the helium dimer as a function of distance using FCI.

3.2 Results and discussion

3.2.1 $(He_2)^+$ dimer

Our first benchmark system is the helium dimer cation. Due to symmetry, the lower and upper charge transfer states, Σ_u^+ and Σ_g^+, feature the charge equally distributed between the helium atoms, and the coupling is simply half of the energy splitting between the two states. The energies and transition dipole moments were computed at intermolecular separations ranging from 2.5 to 6.0 Å. EOM-IP-CCSD and FCI results are presented in Tables 2 and 3, respectively. Figure 13 shows the distance dependence of the FCI coupling. Only basis sets with diffuse functions reproduced the correct exponential decay of the coupling. Without diffuse functions the coupling decays too fast. The magnitude of the coupling is nearly converged at the aug-cc-pVTZ basis.

The convergence of the coupling as a function of the method and the distance is shown in Figure 14. The behavior of the two theoretical methods is essentially

Table 2: Total energy (hartree), energy splitting (cm^{-1}) between Σ_u^+ and Σ_g^+ states, and the transition dipole moment (au) for He_2^+ calculated by EOM-IP-CCSD

	2.50 Å	3.00 Å	4.00 Å	5.00 Å	6.00 Å
cc-pVDZ					
E, hartree	-4.8881821	-4.8832535	-4.8813531	-4.8812386	-4.8812275
ΔE, cm^{-1}	2929.0	824.5	38.73	0.585	0.0026
μ_{tr}	2.348	2.825	3.774	4.721	5.667
aug-cc-pVDZ					
E, hartree	-4.8923633	-4.8868412	-4.8843081	-4.8840117	-4.8839517
ΔE, cm^{-1}	3182.2	990.3	83.2	8.73	0.83
μ_{tr}	2.306	2.795	3.758	4.711	5.660
cc-pVTZ					
E, hartree	-4.9066004	-4.9015533	-4.8994189	-4.8992016	-4.8991721
ΔE, cm^{-1}	3023.5	915.9	74.78	4.30	0.12
μ_{tr}	2.332	2.815	3.769	4.718	5.664
aug-cc-pVTZ					
E, hartree	-4.9077994	-4.9023528	-4.8999136	-4.8996131	-4.8995577
ΔE, cm^{-1}	3125.9	966.7	87.4	7.01	0.70
μ_{tr}	2.307	2.796	3.758	4.711	5.660
d-aug-cc-pVTZ					
E, hartree	-4.9078230	-4.9023713	-4.8999328	-4.8996265	-4.8995691
ΔE, cm^{-1}	3125.1	966.3	87.9	7.33	0.74
μ_{tr}	2.307	2.796	3.758	4.711	5.660
aug-cc-pVQZ					
E, hartree	-4.9106093	-4.9051660	-4.9027398	-4.9024400	-4.9023808
ΔE, cm^{-1}	3117.8	962.8	87.45	7.41	-0.60
μ_{tr}	2.307	2.796	3.758	4.711	5.660
aug-cc-pV5Z					
E, hartree	-4.9114110	-4.9059611	-4.9035383	-4.9032394	-4.9031826
ΔE, cm^{-1}	3115.2	960.8	87.30	7.59	0.60
μ_{tr}	2.307	2.796	3.758	4.711	5.660

identical. Adding the first set of diffuse functions increases the coupling and the magnitude of this effect increases with distance. Further basis set expansion, e.g. adding another set of diffuse or valence functions, have smaller effects. The difference between double-ζ and triple-ζ is significant, but less important than the presence of diffuse functions. One aspect is very interesting — the error of the EOM-IP-CCSD versus FCI decreases at larger distances. We attribute this effect to larger dynamical correlation at shorter distances, i.e., when the distance between electrons is smaller on average. In He_2^+ at large separations, only two electrons need to be correlated

Table 3: Total energy (hartree), energy splitting (cm^{-1}) between Σ_u^+ and Σ_g^+ states, and the transition dipole moment (au) for He_2^+ calculated by FCI

	2.50 Å	3.00 Å	4.00 Å	5.00 Å	6.00 Å
cc-pVDZ					
E, hartree	-4.8882148	-4.8832621	-4.8813536	-4.8812386	-4.8812274
ΔE, cm^{-1}	2939.5	827.5	38.85	0.587	0.0027
μ_{tr}	2.347	2.825	3.774	4.721	5.667
aug-cc-pVDZ					
E, hartree	-4.8926114	-4.8869566	-4.8843362	-4.8840218	-4.8839563
ΔE, cm^{-1}	3219.8	1005.9	85.25	9.04	0.87
μ_{tr}	2.298	2.790	3.755	4.709	5.659
cc-pVTZ					
E, hartree	-4.9066819	-4.9015843	-4.8994248	-4.8992035	-4.8991729
ΔE, cm^{-1}	3039.7	921.6	75.27	4.33	0.12
μ_{tr}	2.330	2.814	3.768	4.717	5.664
aug-cc-pVTZ					
E, hartree	-4.9080572	-4.9024762	-4.8999443	-4.8996242	-4.8995631
ΔE, cm^{-1}	3160.6	981.0	89.02	7.15	0.72
μ_{tr}	2.299	2.790	3.755	4.709	5.658
d-aug-cc-pVTZ					
E, hartree	-4.9080815	-4.9024964	-4.8999652	-4.8996381	-4.8995744
ΔE, cm^{-1}	3159.7	980.9	89.78	7.55	0.77
μ_{tr}	2.299	2.790	3.755	4.709	5.658
aug-cc-pVQZ					
E, hartree	-4.9108665	-4.9052897	-4.9027716	-4.9024514	-4.9023889
ΔE, cm^{-1}	3150.8	976.6	89.17	7.58	0.62
μ_{tr}	2.299	2.790	3.755	4.709	5.658
aug-cc-pV5Z					
E, hartree	-4.9116664	-4.9060840	-4.9035703	-4.9032510	-4.9031878
ΔE, cm^{-1}	3147.5	974.3	89.04	7.77	0.62
μ_{tr}	2.299	2.790	3.755	4.709	5.658

for a good description of dynamical correlation. A similar trend was observed in bond breaking applications of CASSCF and valence optimized orbital coupled cluster doubles (VOO-CCD) methods.[66] Similar trends are observed for the transition dipole moment, as shown in Figure 15. At least a single set of diffuse functions is needed and the values converge at the aug-cc-pVDZ basis set.

For this small benchmark system, we also investigated the performance of methods based on the doublet reference using the aug-cc-pVTZ basis set. These results are given in Table 4. UHF-CIS gives qualitatively incorrect results, i.e. it places the

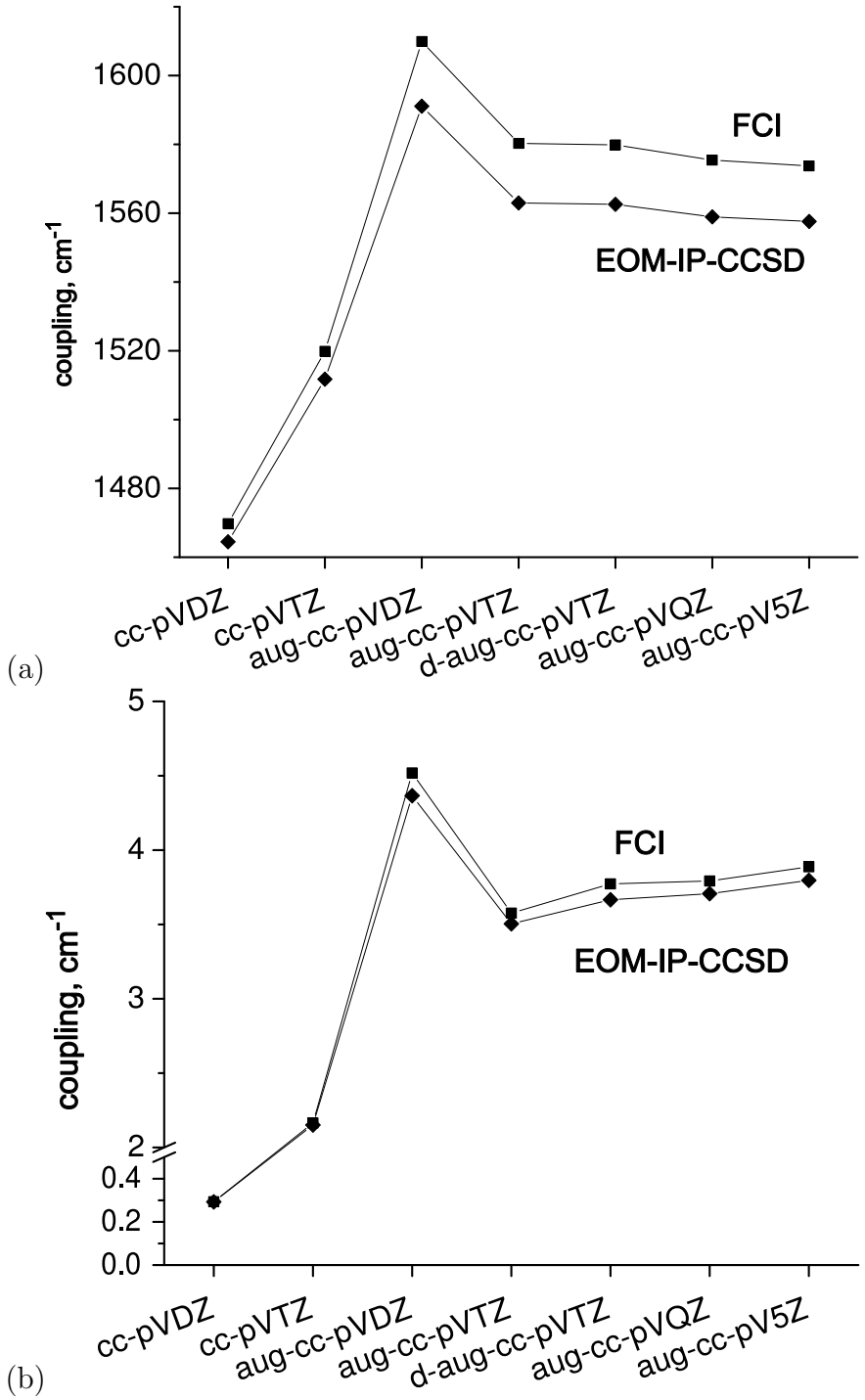

Figure 14: Electronic coupling in He_2^+ at 2.5 Å (a) and 5.0 Å (b) calculated by FCI (squares) and EOM-IP-CCSD (diamonds).

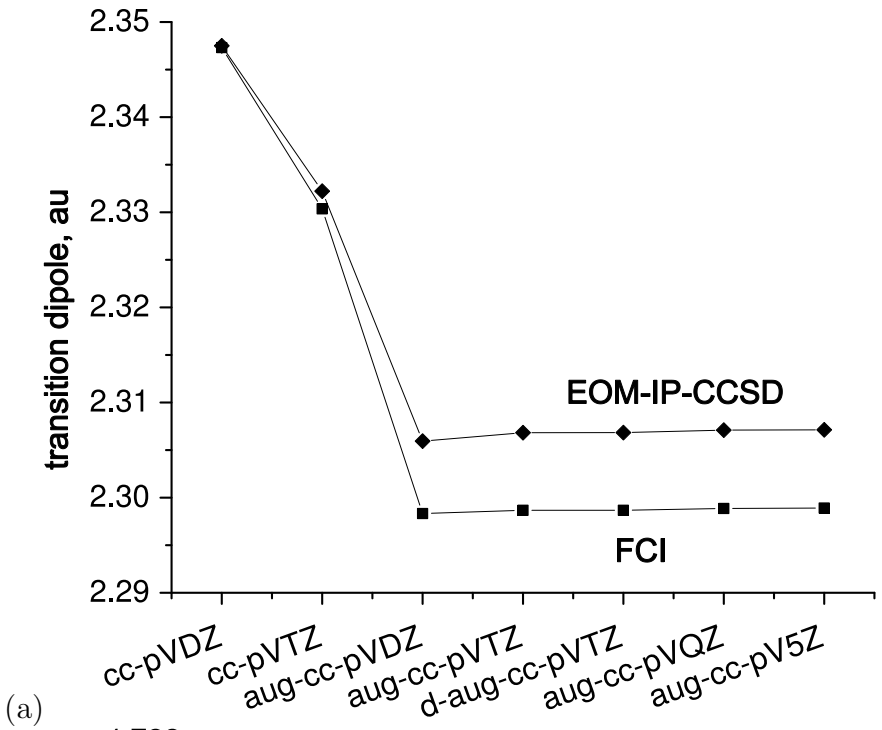

(a)

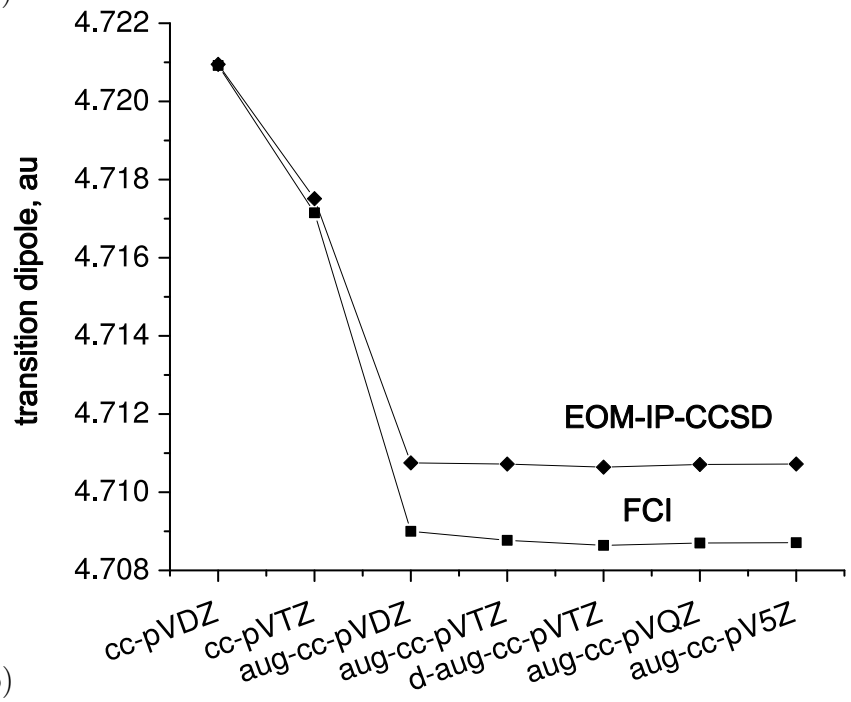

(b)

Figure 15: The transition dipole moment in He_2^+ at 2.5 Å (a) and 5.0 Å (b) calculated by FCI (squares) and EOM-IP-CCSD (diamonds).

Table 4: Total energy (hartree), energy splitting (cm^{-1}) between Σ_u^+ and Σ_g^+ states, and the transition dipole moment (au) for He_2^+ using open-shell reference

	2.50 Å	3.00 Å	4.00 Å	5.00 Å	6.00 Å
HF/CIS	spatial symmetry restricted UHF reference				
E, hartree	-4.8461270	-4.8401184	-4.8373567	-4.8370249	-4.8369709
ΔE, cm^{-1}	-1105.15	-3569.53	-4623.83	-4724.96	-4732.74
μ_{tr}	2.297	2.781	3.735	4.680	5.622
HF/CIS	broken spatial symmetry UHF reference				
E, hartree	-4.8619655	-4.8608400	-4.8603142	-4.8601885	-4.8601448
ΔE, cm^{-1}	21159.45	21201.56	21086.06	21051.22	21039.11
μ_{tr}	0.384	0.150	0.019	0.002	0.0003
q_{gr}, e	0.019	0.008	0.003	0.002	0.001
q_{ex}, e	1.025	0.994	0.996	0.998	0.999
CCSD/EOM-EE-CCSD	spatial symmetry restricted UHF reference				
E, hartree	-4.9077180	-4.9021320	-4.8995985	-4.8992786	-4.8992177
ΔE, cm^{-1}	3007.56	825.27	-66.65	-148.21	-154.48
μ_{tr}	2.299	2.790	3.755	4.709	5.659
CCSD/EOM-EE-CCSD	broken spatial symmetry UHF reference				
E, hartree	-4.9064033	-4.9011883	-4.8997508	-4.8996079	-4.8995614
ΔE, cm^{-1}	3185.51	1365.05	988.34	981.14	979.84
μ_{tr}	2.154	1.995	0.343	0.035	0.004
q_{gr}, e	0.387	0.158	0.005	0.002	0.001
q_{ex}, e	0.686	0.876	0.995	0.998	0.999

excited state below the ground state, and the level splitting does not decay to zero at large distances. This behavior is not rectified by including electron correlation, even at the EOM-EE-CCSD level. The ordering is only correct at small distances; however, the asymptotic distance behavior is still lacking, which is quite unexpected for this 3-electron system.

3.2.2 $(H_2)_2^+$ dimer

The hydrogen dimer cation is isoelectronic with He_2^+; however, due to the additional nuclear degree of freedom the molecular fragments no longer have to be identical, and the charge can be localized. From several possible orientations of the two fragments, we chose a C_{2v} symmetry configuration in which the two molecules are parallel. EOM-IP-CCSD, CCSD/EOM-EE-CCSD, and FCI calculations in the aug-cc-pVTZ basis were performed at reaction coordinate values of 0.0, 0.2, 0.4, 0.45 and 0.5 at 3.0 and

Table 5: Total energy (hartree), energy splitting (cm^{-1}), transition dipole moment (au), ground and excited state charge (au), coupling (cm^{-1}) calculated for $(H_2)_2^+$ at 3.0 Å separation in aug-cc-pVTZ basis set.

	0.0	0.2	0.4	0.45	0.5
FCI					
E, hartree	-1.779004	-1.777154	-1.771929	-1.770939	-1.770563
ΔE, cm^{-1}	15193	9720	5236	4601	4369
μ_{tr}	0.758	1.194	2.226	2.534	2.669
q_{gr},e	0.957	0.924	0.761	0.648	0.500
q_{ex}, e	0.0540	0.0822	0.241	0.353	0.500
h_{ab}, cm^{-1}	2156.2	2174.4	2183.5	2184.4	2184.7
EOM-IP-CCSD					
E, hartree	-1.778861	-1.777017	-1.771813	-1.770830	-1.770456
ΔE, cm^{-1}	15187	9723	5252	4620	4389
μ_{tr}	0.767	1.207	2.243	2.551	2.685
q_{gr},e	0.957	0.924	0.760	0.648	0.500
q_{ex}, e	0.0549	0.0831	0.242	0.354	0.500
h_{ab}, cm^{-1}	2182.4	2196.5	2197.7	2195.7	2194.6
EOM-EE-CCSD					
E, hartree	-1.778942	-1.777015	-1.771434	-1.770244	-1.770200
ΔE, cm^{-1}	15891	10303	5500	4695	4264
μ_{tr}	0.730	1.131	2.077	2.375	2.670
q_{gr},e	0.958	0.930	0.787	0.681	0.500
q_{ex}, e	0.04984	0.06830	0.24243	0.35356	0.500
h_{ab}, cm^{-1}	2167.3	2165.3	2206.5	2186.6	2132.2

5.0 Å separations. The data are summarized in Tables 5 and 6 and the error plots are given in Figure 16 and 17. The EOM-IP-CCSD/aug-cc-pVTZ ionization energies (IEs) are 16.398 and 14.544 eV at neutral and cation geometries, respectively.

A brief explanation of the plots is in order. The errors are calculated as the difference between the approximate value and the exact FCI result. Negative values mean the given quantity is underestimated, while positive values mean the opposite. If the curve is parallel to the x axis, it means that the error is constant throughout the reaction coordinate space, a highly desirable feature. A slope, on the other hand, denotes a change in the quality of description and a non-parallelity error (NPE). The absolute values of the total energy are not important, and only NPEs are of interest — the error for the total energy of the ground state is arbitrarily set to 0 at R=0.

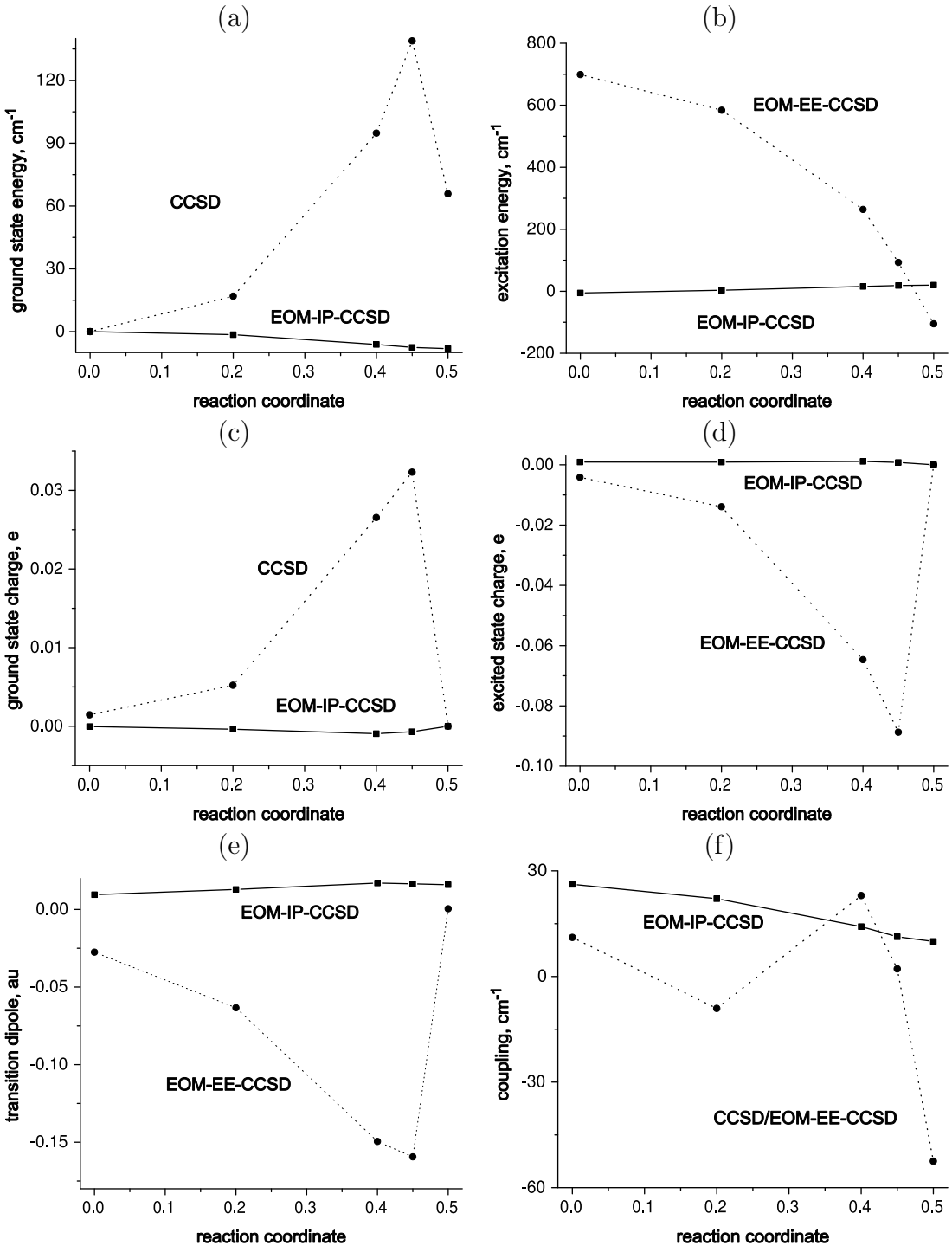

Figure 16: Error in (a) ground state energy, (b) excitation energy, (c) ground state charge, (d) excited state charge, (e) transition dipole moment, and (f) diabatic coupling in $(H_2)^+$ dimer at 3.0 Å separation. EOM-IP-CCSD/aug-cc-pVTZ (solid line) and EOM-EE-CCSD/aug-cc-pVTZ (dotted line) results are shown.

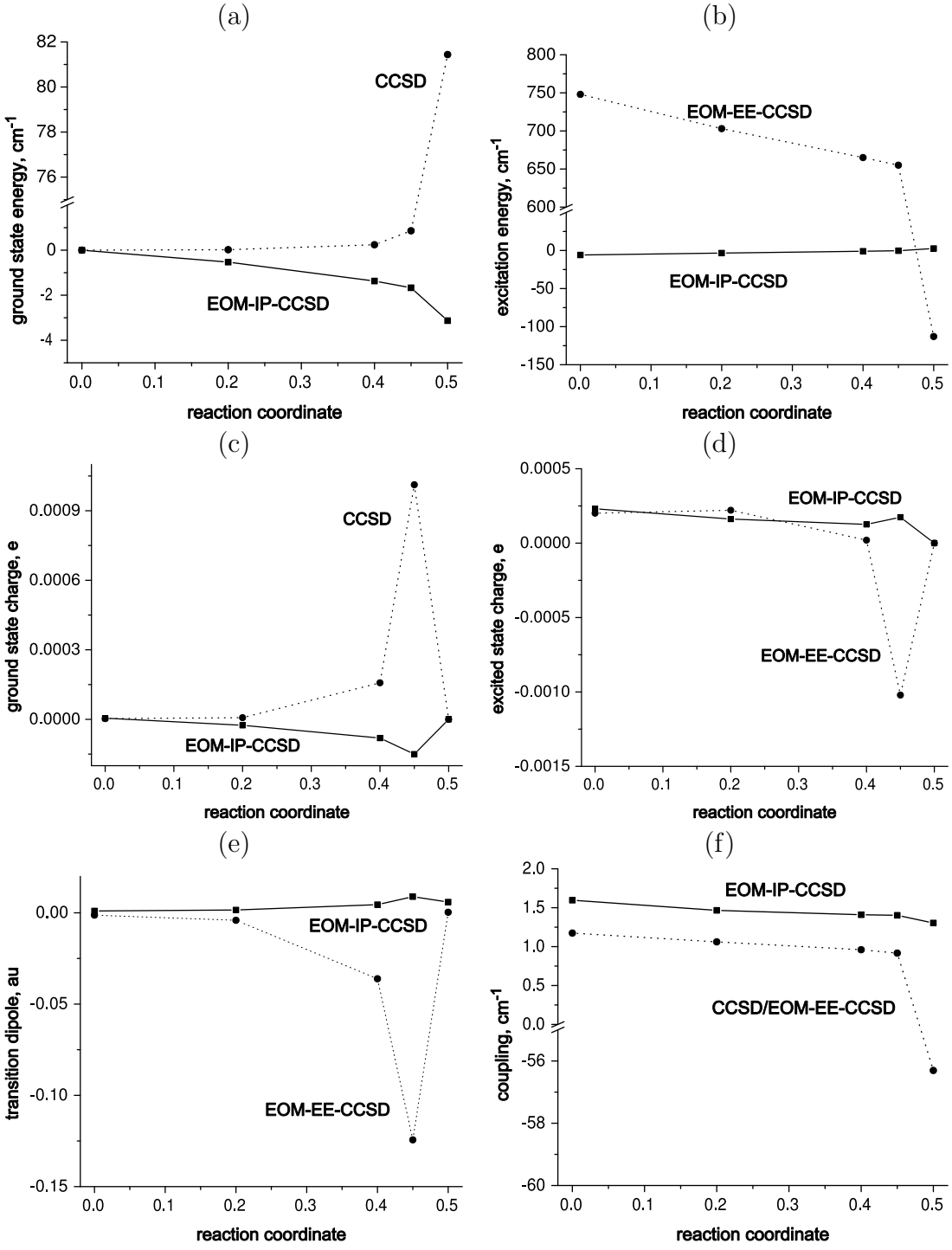

Figure 17: Error in (a) ground state energy, (b) excitation energy, (c) ground state charge, (d) excited state charge, (e) transition dipole moment, and (f) diabatic coupling in $(H_2)^+$ at 5.0 Å separation. EOM-IP-CCSD/aug-cc-pVTZ (solid line) and EOM-EE-CCSD/aug-cc-pVTZ (dotted line) results are shown.

Table 6: Total energy (hartree), energy splitting (cm^{-1}), transition dipole moment (au), ground and excited state charge (au), coupling (cm^{-1}) calculated for $(H_2)_2^+$ at 5.0 Å separation in aug-cc-pVTZ basis set.

	0.0	0.2	0.4	0.45	0.5
FCI					
E, hartree	-1.775487	-1.772451	-1.763942	-1.761042	-1.758121
ΔE, cm^{-1}	14882	8883	2956	1482	133.3
μ_{tr}	0.0412	0.0696	0.210	0.419	4.661
q_{gr},e	0.995	0.994	0.993	0.991	0.500
q_{ex}, e	0.00784	0.00742	0.00739	0.00877	0.500
h_{ab}, cm^{-1}	65.76	66.33	66.60	66.63	66.64
EOM-IP-CCSD					
E, hartree	-1.775475	-1.772442	-1.763936	-1.761037	-1.757504
ΔE, cm^{-1}	14876	8880	2955	1482	135.9
μ_{tr}	0.0422	0.0712	0.215	0.428	4.667
q_{gr},e	0.995	0.994	0.993	0.991	0.500
q_{ex}, e	0.00807	0.00758	0.00751	0.00894	0.50000
h_{ab}, cm^{-1}	67.4	67.8	68.0	68.0	67.9
EOM-EE-CCSD					
E, hartree	-1.775487	-1.772451	-1.763940	-1.761038	-1.757750
ΔE, cm^{-1}	15630	9587	3620	2137	20.7
μ_{tr}	0.040	0.066	0.174	0.295	4.662
q_{gr},e	0.995	0.994	0.993	0.992	0.500
q_{ex}, e	0.00804	0.00764	0.00741	0.00775	0.500
h_{ab}, cm^{-1}	66.9	67.4	67.6	67.5	10.3

For the ground state charge, if the error is positive it signifies that there is excessive charge separation, i.e., the state is overpolarized. Overpolarization of the excited state is manifested by a negative error.

Panels (a) and (b) in Figures 16 and 17 show the error in the ground state total energy and excitation energy, respectively. At small values of R, i.e., when there is large difference between the geometries of the two fragments both methods perform similarly. As the bond lengths become more similar the discrepancy between EOM-EE-CCSD and FCI becomes more significant. Finally, at R=0.5 the doublet HF wave function becomes unstable yielding a cusp on the PES. It is manifested as a large jump on all the plots. Meanwhile the error for EOM-IP-CCSD curves remains small. At 5.0 Å separation and excluding the R=0.5 point, the EOM-EE-CCSD error in

excitation energy ranges between 750 and 650 cm^{-1}. The EOM-IP-CCSD error is confined to the 6 - 0 cm^{-1} range. Similar behavior is observed at 3.0 Å separation. In other words, the EOM-EE-CCSD NPE is high and the description is not uniform throughout the reaction coordinate space.

An important property of a CT system is its charge distribution. Panels (c) and (d) of Figures 16 and 17 show the ground and excited state charge of the more positively charged fragment (in the ground state) at the two interfragment separations. In both cases the EOM-IP-CCSD and FCI results are essentially identical, and the NPE is small. The quality of CCSD/EOM-EE-CCSD description degrades towards R=0.5. Both the ground and excited state become overpolarized as a consequence of the charge-localized character of the UHF doublet reference. The incorrect charge distribution in turn affects the transition dipole moment (Figure 16e, 17e). Again, the EOM-IP-CCSD description is uniform and accurate throughout, while EOM-EE-CCSD underestimates this property.

The calculated couplings depend on the energy splitting, transition and permanent dipole moment of the two states. The values are plotted in panel (f) of Figures 16 and 17. The most striking feature is the cusp of the EOM-EE-CCSD curve at the transition state. It originates from the CCSD PES cusp, as the coupling at this point is equal to half the energy splitting between the two states. EOM-IP-CCSD systematically overestimates the coupling, due to the error in the transition dipole. The coupling weakly depends on the reaction coordinate, in agreement with the Condon approximation, i.e. the coupling only depends on the molecular coordinates that do not affect the effective donor-acceptor distance.

3.2.3 $(Be\text{-}BH)^+$ dimer

The $(Be\text{-}BH)^+$ dimer cation was studied in a linear configuration, with the beryllium atom located on the boron side. aug-cc-pVDZ basis set was used in the calculations.

The data are presented in Table 7 and the error plots are shown in Figure 18. The BH distance was scanned from its cation geometry (R=0) to the neutral geometry (R=1). The distance between the center of mass of both fragments was kept constant at 5.0 Å. EOM-IP-CCSD/aug-cc-pVDZ vertical IE of beryllium is 9.234 eV, while that of BH decreases from 9.687 to 9.679 eV as the bond length increases from the cation to the neutral geometry. The fact that the IE of BH at the cation geometry is larger than at the neutral geometry is due to the fact that the equilibrium bond length were optimized at a different level of theory. It is not a problem in other systems due to larger geometric change. Due to the small changes in the relative energies of both species only subtle changes are expected along the reaction coordinate. Before delving into the details note that both CCSD/EOM-EE-CCSD and EOM-IP-CCSD (in all cases except the ground state energy) capture the trends in properties along the reaction coordinate. The NPE is smaller for EOM-IP-CCSD indicating a more uniform description throughout the reaction coordinate space.

The IEs of both fragments are very close, thus we expect an appreciable extent of charge delocalization. In the ground state roughly 86% of the hole is located on Be, while only 6% in the excited state. Both EOM-IP-CCSD and CCSD predict a slightly more localized structure than FCI, in both states. This in turn affects the transition dipole moment, which decreases as follows: FCI > EOM-IP-CCSD > EOM-EE-CCSD. Clearly, the more charge localized the state is, the lower the transition dipole moment is. The inverse is true for the excitation energies: FCI values are lower than EOM-EE-CCSD, while EOM-IP-CCSD is in-between. Lastly, let us look at the diabatic coupling, which is a cumulative property. Unexpectedly, all methods are in very good accord, within 5%. The agreement for EOM-IP is only slightly inferior than for EOM-EE-CCSD. This is very interesting, as both methods give slightly different picture of the states. In case of EOM-EE-CCSD, the increased transition

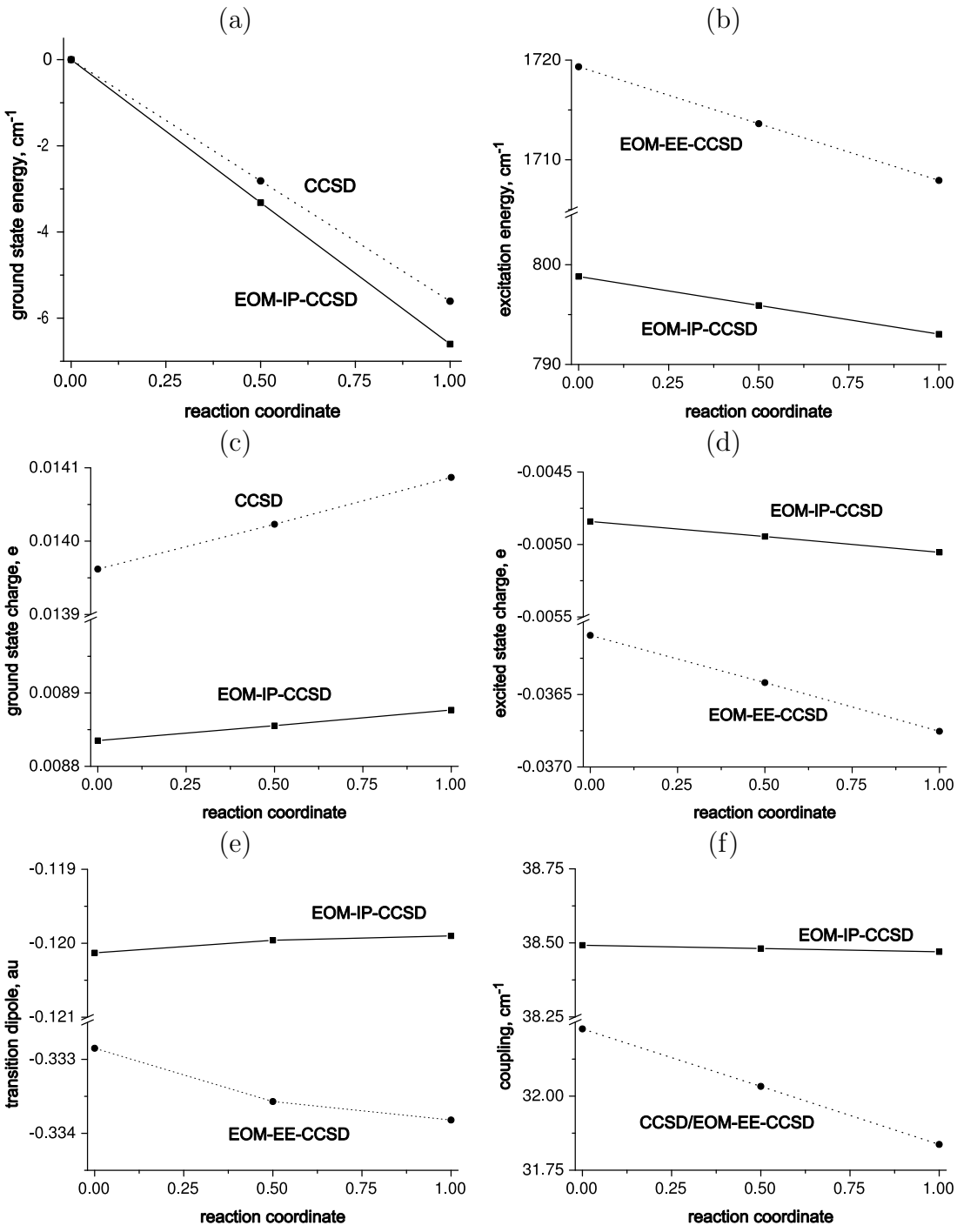

Figure 18: Error in (a) ground state energy, (b) excitation energy, (c) ground state charge, (d) excited state charge, (e) transition dipole moment, and (f) diabatic coupling in $(Be\text{-}BH)^+$. EOM-IP-CCSD/aug-cc-pVDZ (solid line) and EOM-EE-CCSD/aug-cc-pVDZ (dotted line) results are shown. The charge pertains to the Be fragment.

Table 7: Total energy (hartree), energy splitting (cm^{-1}), transition dipole moment (au), ground and excited state charge (au), coupling (cm^{-1}) calculated for linear (Be-BH)$^+$ at 5.0 Å separation in aug-cc-pVDZ basis set. The charge pertains to the Be fragment.

	0.0	0.5	1.0
FCI			
E, hartree	-39.505862	-39.505843	-39.505790
ΔE, cm^{-1}	5295.0	5282.9	5270.6
μ_{tr}, au	1.643	1.647	1.648
q_{gr},e	0.8648	0.8639	0.8630
q_{ex}, e	0.0629	0.0634	0.0639
h_{ab}, cm^{-1}	1053.1	1053.8	1054.5
EOM-IP-CCSD			
E, hartree	-39.506545	-39.506542	-39.506503
ΔE, cm^{-1}	5903.8	5889.0	5873.8
μ_{tr}, au	1.522	1.527	1.528
q_{gr},e	0.8737	0.8728	0.8719
q_{ex}, e	0.0640	0.0645	0.0650
h_{ab}, cm^{-1}	1091.6	1092.3	1093.0
EOM-EE-CCSD			
E, hartree	-39.505518	-39.505513	-39.505472
ΔE, cm^{-1}	6878.9	6861.8	6844.4
μ_{tr}, au	1.310	1.313	1.315
q_{gr},e	0.8788	0.8780	0.8771
q_{ex}, e	0.0451	0.0455	0.0459
h_{ab}, cm^{-1}	1085.4	1085.9	1086.4

energy is compensated by the decreased transition dipole. In the denominator the increased difference in permanent dipole moments compensates for the underestimated transition dipole, see Eq. (36).

3.2.4 (BH-H_2)$^+$ dimer

The BH-H_2 system is an example complementary to Be-BH. The difference in vertical ionization energies is approximately 6 eV, much larger than 0.5 eV in Be-BH. At the cation geometry, the EOM-IP-CCSD/aug-cc-pVDZ IEs of BH and H_2 are 9.687 eV and 14.460 eV, respectively; values at neutral geometries are 9.679 and 16.288 eV. We studied the system in a t-shaped configuration: the H_2 molecule constitutes the top, while BH (boron atom closer to H_2) is the stem. At R=0, H_2 is at its neutral

geometry while BH is at its cation geometry. At R=1, BH is at its neutral geometry, while H_2 is at the cation geometry. The distance between the centers of mass is kept fixed at 3.0 Å. The data are listed in Table 8 and error plots are given in Figure 19. The aug-cc-pVDZ basis set was used in the calculations.

Table 8: Total energy (hartree), energy splitting (cm^{-1}), transition dipole moment (au), ground and excited state charge (au), coupling (cm^{-1}) calculated for t-shaped $(BH\text{-}H_2)^+$ at 3.0 Å separation in aug-cc-pVDZ basis set. The charge pertains to the BH fragment.

	0.0	0.25	0.5	0.75	1.0
FCI					
E, hartree	-26.030624	-26.029212	-26.022318	-26.012228	-26.000430
ΔE, cm^{-1}	48228	44230	40742	37712	35094
μ_{tr}, au	0.6300	0.6842	0.7457	0.8105	0.8761
q_{gr},e	0.998	0.993	0.987	0.981	0.975
q_{ex}, e	0.222	0.220	0.221	0.223	0.226
h_{ab}, cm^{-1}	6643	6592	6612	6652	6694
EOM-IP-CCSD					
E, hartree	-26.028457	-26.027055	-26.020179	-26.010118	-25.998359
ΔE, cm^{-1}	47467	43465	39984	36969	34373
μ_{tr}, au	0.6469	0.7070	0.7733	0.8425	0.9124
q_{gr},e	0.995	0.990	0.984	0.977	0.970
q_{ex}, e	0.214	0.214	0.216	0.219	0.223
h_{ab}, cm^{-1}	6654	6651	6692	6745	6797
EOM-EE-CCSD					
E, hartree	-26.030734	-26.029311	-26.022403	-26.012297	-26.000479
ΔE, cm^{-1}	49088	45053	41523	38448	35783
μ_{tr}, au	0.6273	0.6785	0.7375	0.7998	0.8630
q_{gr},e	0.997	0.992	0.987	0.982	0.976
q_{ex}, e	0.224	0.220	0.219	0.220	0.222
h_{ab}, cm^{-1}	6754	6669	6663	6679	6695

The performance of EOM-IP-CCSD and CCSD/EOM-EE-CCSD is very similar. The errors are smaller for the latter, but the difference is not significant compared to the quantities involved. For instance, at R=0.5 the former underestimates the excitation energy by 750 cm^{-1}, while the latter overestimates it by the same amount. The value of the excitation energy is approximately 40,000 cm $^{-1}$ using all methods. With increased R the energy spacing decreases and CCSD/EOM-EE-CCSD tends to overpolarize both states while EOM-IP-CCSD underpolarizes them. Nonetheless, all

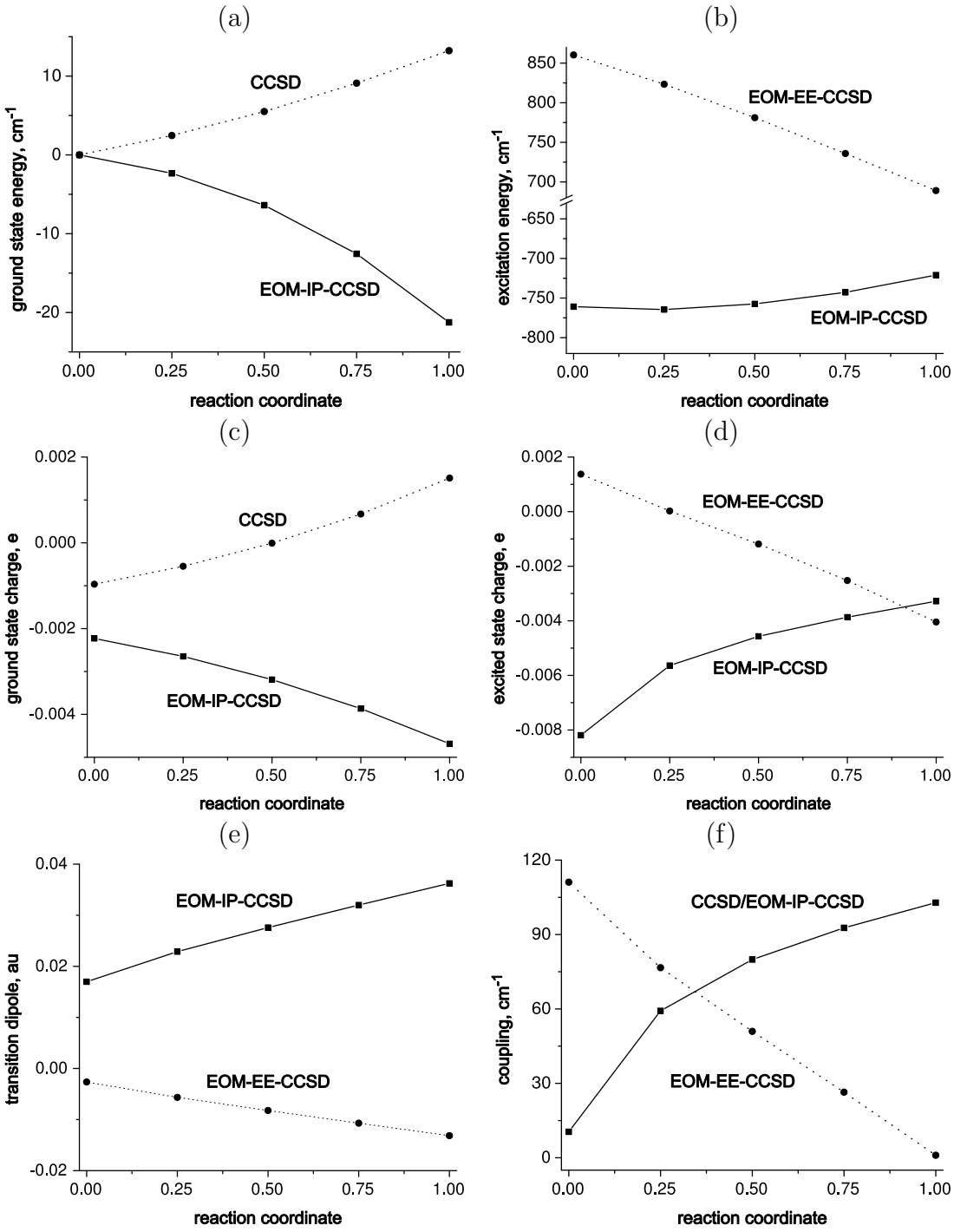

Figure 19: Error in (a) ground state energy, (b) excitation energy, (c) ground state charge, (d) excited state charge, (e) transition dipole moment, and (f) diabatic coupling in $(BH\text{-}H_2)^+$. EOM-IP-CCSD/aug-cc-pVDZ (solid line) and EOM-EE-CCSD/aug-cc-pVDZ (dotted line) results are shown. The charge pertains to the BH fragment.

methods predict the hole to be almost entirely located on BH in the ground state, and on H_2 in the excited state. This is in agreement with the difference of IEs, and according to Eq. 32 signifies a very similar character of diabatic and adiabatic wave functions. Another way of understanding it is by comparing the diabatic coupling with the energy difference between the adiabatic levels. Consider a two-level coupled system. If the two levels are degenerate, they will split by twice the amount for the coupling. In the case, when they are non-degenerate, the amount of splitting induced by the coupling will be less than twice its value. Thus, in $(BH\text{-}H_2)^+$ dimer diabatic coupling can account for utmost 13,000 cm^{-1} of adiabatic state separation. The smallest difference between them occurs at R=1, and is equal to 35,000 cm^{-1}. The difference, 22,000 cm^{-1}, is the difference between energies of the diabatic states. Since it is significantly larger than the coupling, the adiabatic states will be very similar to the diabatic states. This is additionally confirmed by good agreement of transition dipoles between EOM-IP-CCSD and EOM-EE-CCSD. For this molecular system both methods perform similarly and other than the computational cost there is no preference for either one.

3.2.5 $(LiH)_2^+$ dimer

The LiH dimer cation cation was studied in an stacked antiparallel configuration. The separation between the center of mass was held fixed at 4.0 Å. The monomer state considered here corresponds to ionization from the σ bonding orbital of the monomer. According to EOM-IP-CCSD/6-31+G it requires 6.781 and 7.589 eV at the cation and neutral geometries, respectively. The data are listed in Table 9 and error plots are given in Figure 20. The 6-31+G basis set was used in the calculations. The large difference between the IEs causes a significant change in the extent of charge delocalization along the reaction coordinate. This is in stark contrast to BH. Low coupling to Be or H_2 precluded the use of LiH in the heterodimer calculations.

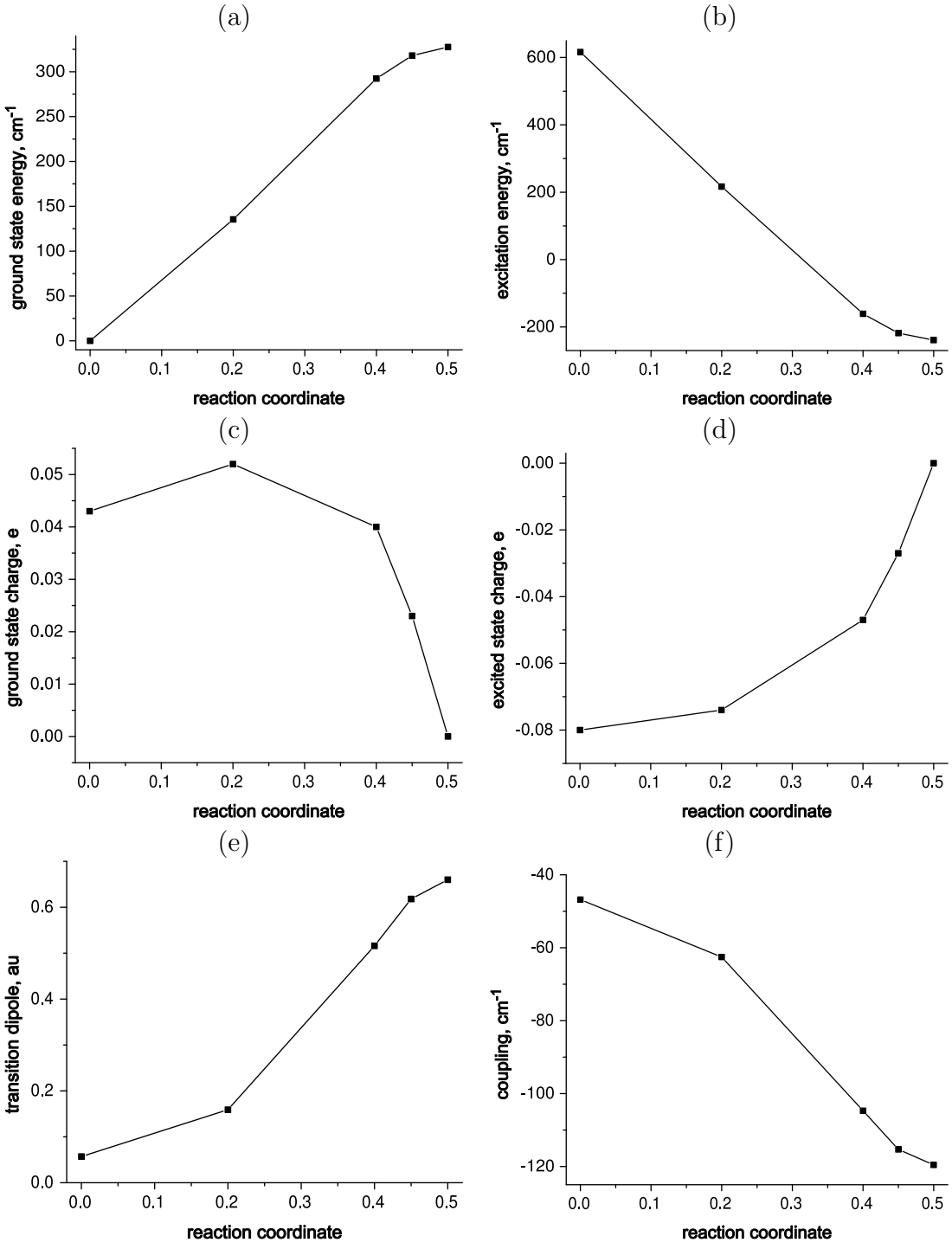

Figure 20: Error in (a) ground state energy, (b) excitation energy, (c) ground state charge, (d) excited state charge, (e) transition dipole moment, and (f) diabatic coupling in $(LiH)_2^+$. EOM-IP-CCSD/6-31+G results are shown.

Panels (a) and (b) of Figure 20 present the error in the ground state total energy and the excitation energy, respectively. There is a significant NPE in both. EOM-IP-CCSD predicts a larger energy change when going from R=0 to R=0.5. At R=0 the excitation energy is overestimated by 600 cm^{-1}, while it is underestimated by 200 cm^{-1} at R=0.5. These numbers do not exceed 10%. FCI yields a less polarized state and a lower transition dipole moment. The error in the transition moment increases as the monomers become more similar. Lastly, EOM-IP-CCSD predicts weaker diabatic coupling than FCI. Note that the NPE is much smaller for the coupling than for the other quantities.

Table 9: Total energy (hartree), energy splitting (cm^{-1}), transition dipole moment (au), ground and excited state charge (au), coupling (cm^{-1}) calculated for $(LiH)_2^+$ at 4.0 Å separation in 6-31+G basis set.

	0.0	0.2	0.4	0.45	0.5
FCI					
E, hartree	-15.7422241	-15.7428853	-15.7420176	-15.7418536	-15.7417941
ΔE, cm^{-1}	6862.5	4924.4	3500.7	3333.3	3275.5
μ_{tr}	1.519	2.131	3.006	3.158	3.214
q_{gr},e	0.845	0.788	0.634	0.570	0.500
q_{ex}, e	0.222	0.252	0.379	0.436	0.500
h_{ab}, cm^{-1}	1661.4	1646.9	1638.8	1638.0	1637.7
EOM-IP-CCSD					
E, hartree	-15.7383087	-15.7383529	-15.7367697	-15.7364888	-15.7363863
ΔE, cm^{-1}	7478.7	5141.0	3339.6	3115.0	3036.3
μ_{tr}	1.576	2.290	3.522	3.776	3.874
q_{gr},e	0.888	0.840	0.674	0.593	0.500
q_{ex}, e	0.141	0.178	0.332	0.410	0.500
h_{ab}, cm^{-1}	1614.6	1584.3	1534.1	1522.7	1518.2

Table 10: Total energy (hartree), energy splitting (cm^{-1}), transition dipole moment (au), ground and excited state charge (au), and coupling (cm^{-1}) calculated for $(C_2H_4)_2^+$ at 4.0 Å separation in 6-31+G basis set.

	0.0	0.2	0.4	0.45	0.5
EOM-IP-CCSD					
E, hartree	-156.078063	-156.079790	-156.080620	-156.080697	-156.080723
ΔE, cm^{-1}	5239	4841	4630	4609	4603
μ_{tr}, au	3.142	3.404	3.561	3.577	3.582
q_{gr},e	0.733	0.652	0.553	0.527	0.500
q_{ex}, e	0.277	0.355	0.450	0.475	0.500
h_{ab}, cm^{-1}	2303.8	2302.6	2301.4	2301.3	2301.3
EOM-IP-CC(2,3)					
E, hartree	-156.083897	-156.085381	-156.086074	-156.086138	-156.086159
ΔE, cm^{-1}	5447	4948	4680	4654	4646
q_{gr},e	0.747	0.663	0.557	0.529	0.500
q_{ex}, e	0.256	0.339	0.443	0.471	0.500
MR-CISD+Q					
E, hartree	-156.077664	-156.079075	-156.079722	-156.079781	-156.079716
ΔE, cm^{-1}	5352	4885	4636	4612	4610
μ_{tr}, au	3.215	3.456	3.597	3.611	3.621
q_{gr},e	0.722	0.643	0.550	0.525	0.500
q_{ex}, e	0.285	0.362	0.452	0.476	0.500
h_{ab}, cm^{-1}	2393.4	2334.6	2305.8	2302.9	2305.2

3.2.6 $(C_2H_4)_2^+$

The results in this section are obtained using 6-31+G basis set. The biggest difference between the neutral and the cation geometry is the C-C bond length: 1.418 and 1.329 Å, respectively. The vertical EOM-IP-CCSD/6-31+G IE of ethylene fragment at neutral geometry is 10.381 eV, while that at the cation geometry is 10.049 eV. We chose the parallel stacked geometry in which the planes of the molecules are separated by 4.0 and 6.0 Å. The results are in Table 10 and Figures 21 and 22.

Figure 21 presents the ground state PES and the charge distribution along the CT reaction coordinate in the ethylene dimer cation are 4 and 6 Å separations. EOM-IP-CCSD produces a smooth change in both quantities, whereas the CCSD curve (using doublet reference) exhibits a cusp at R=0.5. Note that the cusp is present for both UHF and ROHF based curves and is due to unbalanced description of the

important electronic configurations by doublet-reference based CCSD rather than spin contamination of the reference.

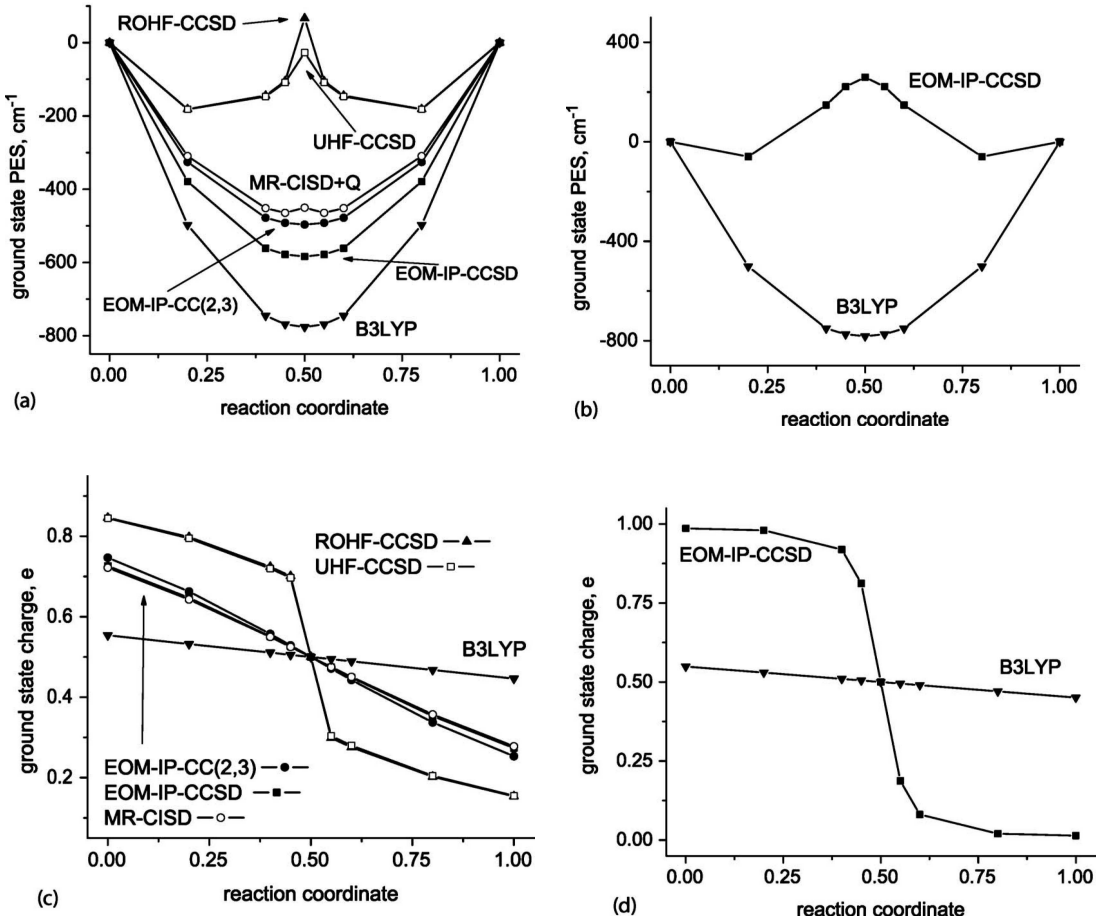

Figure 21: Changes in charge distribution and PES scans along the CT coordinate in the ground state of $(C_2H_4)_2^+$ at 4 Å [panels (a) and (c)] and 6 Å separations [panels (b) and (d)].

Since this system is beyond the reach of FCI, we compare the EOM-IP-CCSD and CCSD/EE-CCSD results against more accurate EOM-IP-CC(2,3) (EOM-IP-CCSD/$3h2p$) values, as well as MR-CISD+Q. As expected, EOM-IP-CC(2,3) and MR-CISD+Q are in an excellent agreement. Both methods predict a deeper potential well, the difference being approximately 100 cm^{-1}. MR-CISD+Q curve has a small cusp due to the frozen core, e.g., the cusp disappears if the excitations from

core orbitals are included at MR-CISD level. Unfortunately,it was not possible to simultaneously unfreeze the core and employ adequately large active space in MRCI calculations.

Overall, EOM-IP-CCSD, EOM-IP-CC(2,3), and MR-CISD predict very similar, smooth changes of the fragment charge. The degree of charge localization is exaggerated in CCSD calculation. This causes an unphysically abrupt change in the polarity of the system around the transition state. Similar discrepancy between EOM-IP-CCSD and EOM-EE-CCSD is present in the excited state.

DFT/B3LYP calculation yields qualitatively correct shapes of the PES at 4 Å; however, the depth and the degree of charge localization are severely overestimated, due to SIE. As the distance between the fragments increases, the R=0.5 point would become a transition state separating to charge-localized minima. At the EOM-IP-CCSD level, this happens at 6 Å, whereas B3LYP still predicts a potential well and significant charge delocalization. In fact, there is only a minor change between the B3LYP results at 4 and 6 Å. Of course, SIE-corrected functionals, e.g., long-range corrected functionals, should be able to better describe these CT systems.

Since the density matrices at the EOM-IP-CC(2,3) level are not available, we have restricted ourselves to the calculation of energies and permanent dipoles via finite differences. All differences shown in Figure 22 were calculated relative to EOM-IP-CC(2,3).

As is evident from Figure 22(a), the depth of the potential well along R is overestimated by EOM-IP-CCSD. The largest error is 80 cm^{-1} and occurs at R=0.5. This is best compared to the excitation energy, which at this point is 4603 cm^{-1}. The Mr-CISD+Q/EOM-IP-CC(2,3) difference is approximately half of the EOM-IP-CCSD error. The error in the excitation energy is shown in Figure 22(b). For EOM-IP-CCSD it decreases toward the transition state from 200 to 50 cm^{-1}. In other words, the quality of the EOM-IP-CCSD wave function improves as the monomers become

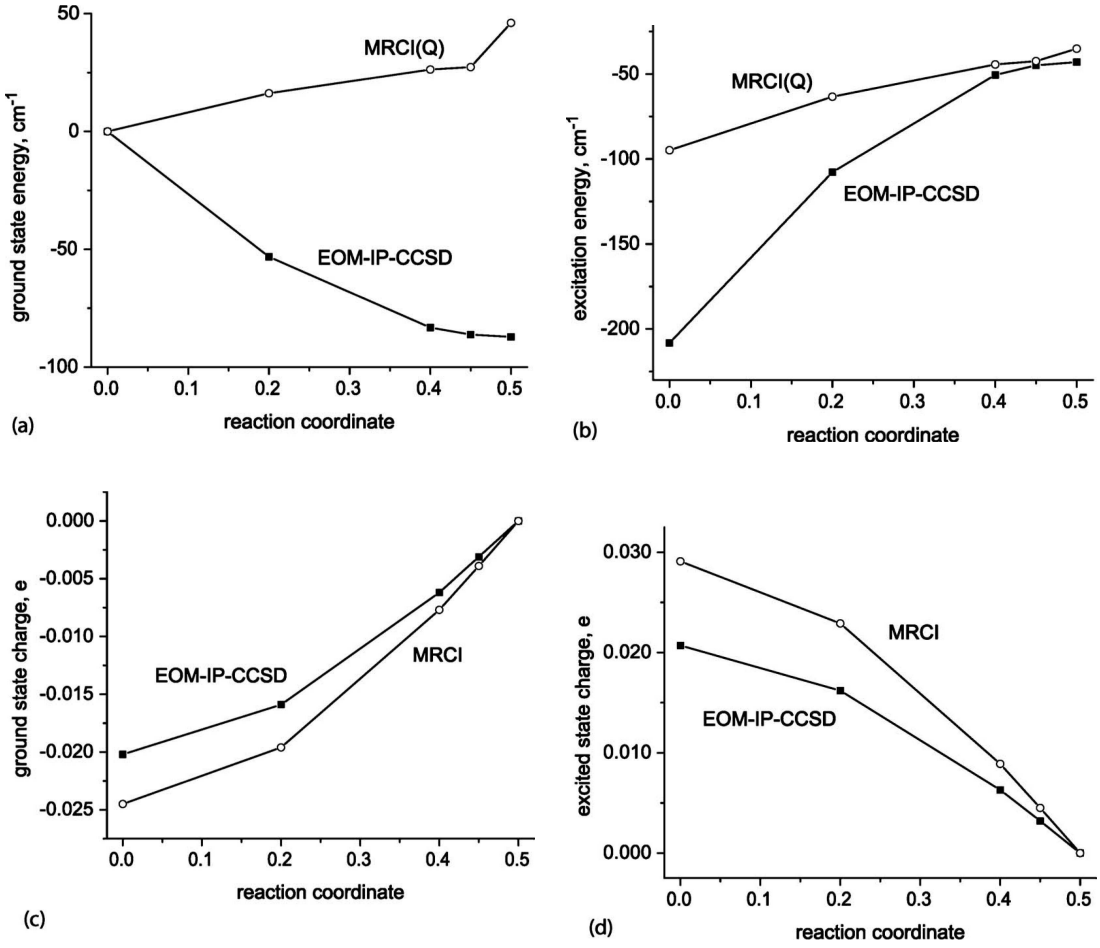

Figure 22: Differences against EOM-IP-CCSD($3h2p$) for (a) ground state energy, (b) excitation energy, (c) ground state charge, and (d) excited state charge in $(C_2H_4)_2^+$. EOM-IP-CCSD/6-31+G results are shown.

more similar; however, NPE is appreciable. Figures 22(c) and 22(d) show the ground and excited state charge. In both cases, the EOM-IP-CCSD and MR-CISD methods underpolarize the CT state relative to EOM-IP-CC(2,3). The magnitude of the difference is small thus yielding credence to the transition dipole moment. As seen previously, exaggerated delocalization leads to transition dipole moments that are typically too high. The diabatic coupling varies smoothly with R. The lack of EOM-IP-CC(2,3) transition dipole prevents us from making a direct comparison of the diabatic coupling. In other systems studied we have witnessed a peculiar error cancellation between ingredients of Eq. (36), which gives us confidence in the presented values. A comparison between MRCI and EOM-IP-CCSD is very interesting. Quantitatively the results are very similar. Note, however, that while EOM-IP-CCSD coupling changes by 2 cm^{-1} between R=0 and R=0.5, MRCI predicts a 90 cm^{-1} change.

3.3 Conclusions

The presented results demonstrate that EOM-IP-CCSD is a reliable method for the study of noncovalent ionized dimers. It yields smooth variation of energies and molecular properties with nuclear coordinates. Most importantly, the cusp in the PES along charge transfer coordinates that is associated with the open-shell reference is completely avoided. Also, the NPE is typically small. In other words, different spatial arrangements of the fragments are described with equal accuracy. The advantages of the EOM-IP method become even more important when the ionized states of the monomers feature electronic degeneracies, as in benzene dimer cation.[96]

In cases where the difference in IEs is much larger than the coupling, EOM-IP-CCSD and EOM-EE-CCSD perform similarly. Due to the lower computational scaling, the former method is preferable. An argument can be made that just like

EOM-EE-CCSD overpolarizes the states, the EOM-IP-CCSD method may appreciably underpolarize the states. In the studied systems only a small degree of underpolarization has been observed. The diabatic coupling has proved to be a fairly insensitive probe of the quality of state description. The increased polarity of EOM-EE-CCSD states is offset by lower transition dipoles and higher excitation energies. Comparison of transition dipole moments offers a better one-number descriptor of the quality of the ground and excited state wave functions.

We expect that the presented results will provide useful calibration data for calculation of electronic coupling elements as well as dimer properties.

CHAPTER IV

CONCLUSION

This thesis presents two stories about exploring different chemical systems and methods in quantum mechanics. In the second chapter, substituent effects in π-π interactions are studied. The third chapter is an exploration of radical cation dimers. Both chapters involve a study of high-level quantum mechanical methods and the approximations that can be made to reduce computational cost while retaining accuracy.

In chapter two, the fundamental nature of substituent interactions on π-π systems was explored. Several computational methods were compared and contrasted before the physics behind these interactions was studied. MP2 theory overestimates the binding energy of all the systems studied. However, when MP2 is combined with the truncated aug-cc-pVDZ basis set (ADZ'), the cancellation of error between an incomplete description of the wavefunction and the approximate description of electron correlation means that this level of theory compares well with CCSD(T). It is important to mention that MP2/ADZ' cannot be applied reliably to all systems, because the approximations are not guaranteed to cancel each other. The spin-component scaled MP2 (SCS-MP2) on the other hand is a systematic approach that can be applied to other π-π systems. SCS-MP2 was found to reliably model π-π interactions in the systems studied.

The nature of the substituent effect was studied in detail for several different types of substituents in a variety of geometries. The binding of the dimers studied was attributed to both an influence of the substituent on the electronic structure of the benzene ring and a direct substituent-π interaction. The computations showed that

polarizable substituents, such as cyano and hydroxyl groups, increase dispersive interactions with the aromatic ring. Substituents such as fluorine decrease binding when displaced toward an electron rich π-cloud due to unfavorable electrostatic interactions. Substituents always increase the binding energy of benzene dimer in displaced edgewise configurations.

In chapter three, the most exact theory available in quantum chemistry, full configuration interaction, was applied to small radical cation dimer systems. Several different systems were studied in a variety of orientations. These calculations where then used to quantitatively determine the error introduced by the EOM methods. EOM-IP-CCSD was determined to perform the most reliably among the methods studied. The success of the EOM-IP-CCSD method is attributed to starting with a reference wavefunction that does not suffer from symmetry breaking. The stability of the reference wavefunction provides smooth energies and stable molecular properties across the CT coordinate. EOM-EE-CCSD can perform similarly to EOM-IP-CCSD if the difference in ionization energy of the two fragments is large. In this case, EOM-IP-CCSD is preferred due to better scaling.

Future work could be done in three specific areas. An extension of the π-π study would involve looking at additional types of substituents and multiple substituents in parallel displaced orientations. In addition, it would be of interest to study how different types of substituents on the same ring influence the π-π interaction. For example, how is the π-π interaction affected by placing an electron-donating and electron-withdrawing group on the same benzene ring? The knowledge gained from studying π-π interactions further is essential for the development of new pharmaceuticals and understanding the fundamental nature of interactions present in biochemistry. The radical cation study showed that EOM-IP-CCSD can be used reliably. The EOM-IP-CCSD method could be applied to other interesting charge transfer systems. Further studies of charge transfer in DNA base pairs could greatly enhance

our understanding of DNA damage repair processes. Charge transfer is a fundamental process in many molecular devices, including organic semiconductors. Studies on polymers and organic molecules could lead to better devices for solar power and organic light-emitting diodes. Together, the insight gained from the two studies in this thesis could point the way to studies of substituent effects in charged π-π systems. Substituents are know to enhance π-π interactions; however, it is not known exactly how substituents would simultaneously affect both charge transfer and the π-π interaction.

REFERENCES

[1] Achiba, Y., Tomoda, S., and Kimura, K. *Chem. Phys. Lett.*, vol. 87, p. 197, 1982.

[2] Adams, H., Carver, F. J., Hunter, C. A., Morales, J. C., and Seward, E. M., "Chemical double-mutant cycles for the measurement of weak intermolecular interactions: Edge-to-face aromatic interactions," *Angew. Chem. Int. Ed. Engl.*, vol. 35, no. 13/14, pp. 1542–1544, 1996.

[3] Alexander, M. H. *J. Chem. Phys.*, vol. 99, p. 6014, 1993.

[4] Almlöf, O. V. and Feyereisen, M. W. *Chem. Phys. Lett.*, vol. 213, p. 514, 1993.

[5] Amini, A. and Harriman, A. *J. Photochem. Photobiol.*, vol. 4, p. 155, 2003.

[6] Arnstein, S. A. and Sherrill, C. D. *Phys. Chem. Chem. Phys.*, vol. 10, p. 2646, 2008.

[7] Bally, T. and Sastry, G. N., "Incorrect dissociation behavior of radical ions in density functional calculations," *J. Phys. Chem. A*, vol. 101, pp. 7923–7925, 1997.

[8] Bartlett, R. J. *Int. J. Mol. Sci.*, vol. 3, p. 579, 2002.

[9] Bartlett, R. J. and Stanton, J. F. *Rev. Comp. Chem.*, vol. 5, p. 65, 1994.

[10] Becke, A. D. *J. Chem. Phys.*, vol. 98, p. 5648, 1993.

[11] Boys, S. F. and Bernardi, F., "The calculation of small molecular interactions by the differences of separate total energies. Some procedures with reduced errors," *Mol. Phys.*, vol. 19, no. 4, pp. 553–566, 1970.

[12] Bukowski, R., Cencek, W., Jankowski, P., Jeziorski, B., Jeziorska, M., Kucharski, S. A., Lotrich, V. F., Misquitta, A. J., Moszynski, R., Patkowski, K., Rybak, S., Szalewicz, K., Williams, H. L., Wheatley, R. J., Wormer, P. E. S., and Zuchowski, P. S., "SAPT2006: An ab initio program for many-body symmetry-adapted perturbation theory calculations of intermolecular interaction energies. see: http://www.physics.udel.edu/∼szalewic/SAPT.."

[13] Bukowski, R., Cencek, W., Jankowski, P., Jeziorski, B., Jeziorska, M., Kucharski, S. A., Misquitta, A. J., Moszynski, R., Patkowski, K., Rybak, S., Szalewicz, K., Williams,

H. L., and Wormer, P. E. S., "SAPT2002: An ab initio program for many-body symmetry-adapted perturbation theory calculations of intermolecular interaction energies. sequential and parallel versions. see: http://www.physics.udel.edu/∼szalewic/SAPT/SAPT.html.."

[14] Burley, S. K. and Petsko, G. A., "Aromatic-aromatic interaction: A mechanism of protein structure stabilization," *Science*, vol. 229, pp. 23–28, 1985.

[15] C. Petrongolo, G. H. and Buenker, R. J. *Mol. Phys.*, vol. 70, p. 825, 1990.

[16] Carra, C., Iordanova, N., and Hammes-Schiffer, S. *J. Phys. Chem. B.*, vol. 106, p. 8415, 2002.

[17] Carver, F. J., Hunter, C. A., Livingstone, D. J., McCabe, J. F., and Seward, E. M., "Substituent effects on edge-to-face aromatic interactions," *Chem. Eur. J.*, vol. 8, no. 13, pp. 2848–2859, 2002.

[18] Cave, R. J. and Newton, M. D. *Chem. Phys. Lett.*, vol. 249, p. 15, 1996.

[19] Cave, R. J. and Newton, M. D. *J. Chem. Phys.*, vol. 106, p. 9213, 1997.

[20] Chaudhuri, R., Mukhopadhyay, D., and Mukherjee, D. *Chem. Phys. Lett.*, vol. 162, p. 393, 1989.

[21] Cockroft, S. L., Hunter, C. A., Lawson, K. R., Perkins, J., and Urch, C. J., "Electrostatic control of aromatic stacking interactions," *J. Am. Chem. Soc.*, vol. 127, p. 8594, 2005.

[22] Cockroft, S. L., Perkins, J., Zonta, C., Adams, H., Spey, S. E., Low, C. M. R., Vinter, J. G., Lawson, K. R., Urch, C. J., and Hunter, C. A., "Substituent effects on aromatic stacking interactions," *Org. Biomol. Chem.*, vol. 5, p. 1062, 2007.

[23] Cohen, R. D. and Sherrill, C. D. *J. Chem. Phys.*, vol. 114, p. 8257, 2001.

[24] Collings, J. C., Roscoe, K. P., Robins, E. G., Batsanov, A. S., Stimson, L. M., Howard, J. A. K., Clark, S. J., and Marder, T. B., "Arene-perfluoroarene interactions in crystal engineering 8: structures of 1:1 complexes of hexafluorobenzene with fused-ring polyaromatic hydrocarbons," *New J. Chem.*, vol. 26, p. 1740, 2002.

[25] Cozzi, F., Cinquini, M., Annuziata, R., Dwyer, T., and Siegel, J. S., "Polar/π interactions between stacked aryls in 1,8-diarylnaphthalenes," *J. Am. Chem. Soc.*, vol. 114, no. 14, pp. 5729–5733, 1992.

[26] Cozzi, F., Ponzini, F., Annunziata, R., Cinquini, M., and Siegel, J. S., "Polar interactions between stacked π systems in fluorinated 1,8-diarylnaphthalenes: Importance of quadrupole moments in molecular recognition," *Angew. Chem. Int. Ed. Engl.*, vol. 34, no. 9, pp. 1019–1020, 1995.

[27] Cozzi, F. and Siegel, J. S., "Interaction between stacked aryl groups in 1,8-diarylnaphthalenes: Dominance of polar/π over charge-transfer effects," *Pure and Appl. Chem.*, vol. 67, no. 5, pp. 683–689, 1995.

[28] Crawford, T. D., Sherrill, C. D., Valeev, E. F., Fermann, J. T., King, R. A., Leininger, M. L., Brown, S. T., Janssen, C. L., Seidl, E. T., Kenny, J. P., and Allen, W. D. *J. Comput. Chem.*, vol. 28, p. 1610, 2007.

[29] Davidson, E. R. and Borden, W. T. *J. Phys. Chem.*, vol. 87, p. 4783, 1983.

[30] de Visser, S. P., de Koning, L. J., and Nibbering, N. M. M. *J. Phys. Chem.*, vol. 99, p. 15444, 1995.

[31] DeFrees, D. J. and McLean, A. D. *J. Chem. Phys.*, vol. 81, p. 3353, 1984.

[32] Delaney, S. and Barton, J. K. *J. Org. Chem.*, vol. 68, p. 6475, 2003.

[33] Dobbyn, A. J. and Knowles, P. J. *Mol. Phys.*, vol. 91, p. 6014, 1993.

[34] Dreuw, A. and Head-Gordon, M. *Chem. Rev.*, vol. 105, p. 4009, 2005.

[35] Dreuw, A. and Head-Gordon, M. *Chem. Phys. Lett.*, vol. 426, p. 231, 2006.

[36] Eisfeld, W. and Morokuma, K. *J. Chem. Phys.*, vol. 113, p. 5587, 2000.

[37] Emrich, K. *Nucl. Phys.*, vol. A351, p. 379, 1981.

[38] EMSL, "Basis sets were obtained from the Extensible Computational Chemistry Environment Basis Set Database, Version , as developed and distributed by the Molecular Science Computing Facility, Environmental and Molecular Sciences Laboratory which is part of the Pacific Northwest Laboratory, P.O. Box 999, Richland, Washington 99352, USA, and funded by the U.S. Department of Energy. The Pacific Northwest Laboratory is a multi-program laboratory operated by Battelle Memorial Institue for the U.S. Department of Energy under contract DE-AC06-76RLO 1830. Contact David Feller or Karen Schuchardt for further information.."

[39] Endres, R. G., Cox, D. L., and Singh, R. R. P. *Rev. Mod. Phys.*, vol. 76, p. 195, 2004.

[40] Enomoto, K., LaVerne, J. A., , and Araos, M. S. *J. Phys. Chem. A*, vol. 111, p. 9, 2007.

[41] Ferguson, E. E., Fehsenfield, F. C., and Albritton, D. L. *Gas Phase Ion Chemistry*, vol. 1, p. 45, 1979.

[42] Gary, H. B. and Winkler, J. R. *Q. Rev. Biophys.*, vol. 36, p. 341, 2003.

[43] Geertsen, J., Rittby, M., and Bartlett, R. J. *Chem. Phys. Lett.*, vol. 164, p. 57, 1989.

[44] Grimme, S., "Improved second-order møller-plesset perturbation theory by separate scaling of parallel- and antiparallel-spin pair correlation energies," *J. Chem. Phys.*, vol. 118, no. 20, pp. 9095–9102, 2003.

[45] Grover, J. R., Walters, E. A., and Hui, E. T. *J. Phys. Chem.*, vol. 91, p. 3233, 1987.

[46] Gung, B. W. and Amicangelo, J. C., "Substituent effects in C_6H_6-C_6H_5X stacking interactions," *J. Org. Chem.*, vol. 71, pp. 9261–9270, 2006.

[47] Gung, B. W., Xue, X., and Reich, H. J., "The strength of parallel-displaced arene-arene interactions in chloroform," *J. Org. Chem.*, vol. 70, pp. 3641–3644, 2005.

[48] Hiberty, P. C., Humbel, S., Danovich, D., and Shaik, S. *J. Am. Chem. Soc.*, vol. 117, p. 9003, 1995.

[49] Hill, J. G. and Platts, J. A., "Spin-component scaling methods for weak and stacking interactions," *J. Chem. Theory Comput.*, vol. 3, pp. 80–85, 2007.

[50] Hobza, P., Selzle, H. L., and Schlag, E. W., "Potential energy surface for the benzene dimer. results of *ab initio* CCSD(T) calculations show two nearly isoenergetic structures: T-shaped and parallel-displaced," *J. Phys. Chem.*, vol. 100, pp. 18790–18794, 1996.

[51] Illies, A. J., McKee, M. L., and Schlegel, H. B. *J. Phys. Chem.*, vol. 91, p. 91, 1987.

[52] Inokuchi, Y., Y. Naitoh, K. O., Saitow, K., Yoshihara, K., and Nishi, N. *Chem. Phys. Lett.*, vol. 269, p. 298, 1997.

[53] Jaffe, R. L. and Smith, G. D., "A quantum chemistry study of benzene dimer," *J. Chem. Phys.*, vol. 105, pp. 2780–2788, 1996.

[54] Jensen, F., *Introduction to Computational Chemistry*. Wiley, 1999.

[55] Jeziorski, B., Moszynski, R., and Szalewicz, K., "Perturbation theory approach to intermolecular potential energy surfaces of van der waals complexes," *Chem. Rev.*, vol. 94, pp. 1887–1930, 1994.

[56] Jungwirth, P. and Bally, T. *J. Am. Chem. Soc.*, vol. 115, p. 5783, 1993.

[57] Kamyia, M. and Hirata, S. *J. Chem. Phys.*, vol. 125, p. 074111, 2006.

[58] Kendall, R. A., Dunning, T. H., and Harrison, R. J., "Electron affinities of the first-row atoms revisited. systematic basis sets and wave functions," *J. Chem. Phys.*, vol. 96, pp. 6796–6806, 1992.

[59] Kim, E., Paliwal, S., and Wilcox, C. S., "Measurements of molecular electrostatic field effects in edge-to-face aromatic interactions and CH-π interactions with implications for protein folding and molecular recognition," *J. Am. Chem. Soc.*, vol. 120, pp. 11192–11193, 1998.

[60] Koch, H., Jørgen Aa. Jensen, H., Jørgensen, P., and Helgaker, T. *J. Chem. Phys.*, vol. 93, p. 3345, 1990.

[61] Kong, J., White, C. A., Krylov, A. I., Sherrill, C. D., Adamson, R. D., Furlani, T. R., Lee, M. S., Lee, A. M., Gwaltney, S. R., Adams, T. R., Daschel, H., Zhang, W., Korambath, P. P., Ochsenfeld, C., Gilbert, A. T. B., Kedziora, G. S., Maurice, D. R., Nair, N., Shao, Y., Besley, N. A., Maslen, P. E., Dombrowski, J. P., Baker, J., Byrd, E. F. C., Voorhis, T. V., Oumi, M., Hirata, S., Hsu, C.-P., Ishikawa, N., Florian, J., Warshel, A., Johnson, B. G., Gill, P. M. W., Head-Gordon, M., and Pople, J. A., "Q-Chem 2.0: A high performance ab initio electronic structure program package," *J. Comput. Chem.*, vol. 21, pp. 1532–1548, 2000.

[62] Kowalski, K. and Piecuch, P. *J. Chem. Phys.*, vol. 115, p. 643, 2001.

[63] Krause, H., Ernstberger, B., and Neusser, H. J. *Chem. Phys. Lett.*, vol. 184, p. 411, 1991.

[64] Krylov, A. I. *Chem. Phys. Lett.*, vol. 338, p. 375, 2001.

[65] Krylov, A. I. *Acc. Chem. Res.*, vol. 39, p. 83, 2006.

[66] Krylov, A. I., C. D. Sherrill, C., Byrd, E. F. C., and Head-Gordon, M. *J. Chem. Phys.*, vol. 109, p. 10669, 1998.

[67] Langhoff, S. R. and Davidson, E. R., "Configuration interaction calculations on the nitrogen molecule," *Int. J. Quantum Chem.*, vol. 8, p. 61, 1974.

[68] Lee, E. C., Hong, B. H., Lee, J. Y., Kim, J. C., Kim, D., Kim, Y., Tarakeshwar, P., and Kim, K. S., "Substituent effects on edge-to-face aromatic interactions," *J. Am. Chem. Soc.*, vol. 127, pp. 4530–4537, 2005.

[69] Lee, E. C., Kim, D., Jurečka, P., Tarakeshwar, P., Hobza, P., and Kim, K. S., "Understanding of assembly phenomena by aromatic-aromatic interactions: Benzene dimer and substituted systems," *J. Phys. Chem. A*, vol. 111, p. 3446, 2007.

[70] Levchenko, S. V. and Krylov, A. I. *J. Chem. Phys.*, vol. 120, p. 175, 2004.

[71] Levchenko, S. V., Wang, T., and Krylov, A. I. *J. Chem. Phys.*, vol. 122, p. 224106, 2005.

[72] Leys, D., Meyer, T. E., Tsapin, A. S., Nealson, K. H., Cusanovich, M. A., and Van Beeumen, J. J. *J. Biol. Chem.*, vol. 277, p. 35703, 2002.

[73] Lindh, R. and Barnes, L. A. *J. Chem. Phys.*, vol. 100, p. 224, 1994.

[74] Löwdin, P. O. *Rev. Mod. Phys.*, vol. 35, p. 496, 1963.

[75] Lundber, M. and Siegbahn, P. E. M. *J. Chem. Phys.*, vol. 122, p. 224103, 2005.

[76] Macías, A. and Riera, A. *J. Phys. B*, vol. 11, p. L489, 1978.

[77] Malar, E. J. P. and Chandra, A. K. *J. Phys. Chem.*, vol. 85, p. 2190, 1981.

[78] Marcus, R. A. *Discussions Faraday Soc.*, vol. 29, p. 21, 1960.

[79] Marcus, R. A. *J. Chem. Phys.*, vol. 43, p. 679, 1965.

[80] Marcus, R. A. *Biochim. Biophys. Acta*, vol. 811, p. 265, 1985.

[81] Mead, C. A. and Truhlar, D. G. *J. Chem. Phys.*, vol. 77, p. 6090, 1982.

[82] Meissner, L. and Bartlett, R. J. *J. Chem. Phys.*, vol. 94, p. 6670, 1991.

[83] Meyer, E. A., Castellano, R. K., and Diederich, F., "Interactions with aromatic rings in chemical and biological recognition," *Angew. Chem. Int. Ed. Engl.*, vol. 42, no. 11, pp. 1210–1250, 2003.

[84] Nakatsuji, H. *Chem. Phys. Lett.*, vol. 177, p. 331, 1991.

[85] Nakatsuji, H. and Hirao, K. *J. Chem. Phys.*, vol. 68, p. 2053, 1978.

[86] Newton, M. *Chem. Rev.*, vol. 91, p. 767, 1991.

[87] Nooijen, M. and Bartlett, R. J. *J. Chem. Phys.*, vol. 102, p. 3629, 1995.

[88] Norris, J. R., Uphaus, R. A., Crespi, H. L., and Katz, J. *Proc. Natl. Acad. Sci.*, vol. 68, p. 625, 1971.

[89] Ohashi, K., Nakai, Y., Shibata, T., and Nishi, N. *Laser Chem.*, vol. 14, p. 3, 1994.

[90] Okamoto, K., Saeki, A., Kozawa, T., Yoshida, Y., and Tagawa, S. *Chem. Lett.*, vol. 2003, p. 834, 2003.

[91] Olsen, J. *J. Chem. Phys.*, vol. 113, p. 7140, 2000.

[92] Pal, S., Rittby, M., Bartlett, R. J., Sinha, D., and Mukherjee, D. *Chem. Phys. Lett.*, vol. 137, p. 273, 1987.

[93] Paliwal, S., Geib, S., and Wilcox, C. S., "Molecular torsion balance for weak molecular recognition forces. effects of "tilted-t" edge-to-face aromatic interactions on conformational selection and solid-state structure," *J. Am. Chem. Soc.*, vol. 116, pp. 4497–4498, 1994.

[94] Piecuch, P. and Bartlett, R. J. *Adv. Quantum Chem.*, vol. 34, p. 295, 1999.

[95] Pieniazek, P. A., Arnstein, S. A., Bradforth, S. E., Krylov, A. I., and Sherrill, C. D., "Benchmark full configuration interaction and equation-of-motion coupled-cluster model with single and double substitutions for ionized systems results for prototypical charge," *J. Chem. Phys.*, vol. 127, p. 164110, 2007.

[96] Pieniazek, P. A., Krylov, A. I., and Bradforth, S. E. *J. Chem. Phys.*, vol. 127, p. 044317, 2007.

[97] Pluháčková, K., Jurečka, P., , and Hobza, P. *Phys. Chem. Chem. Phys.*, vol. 9, p. 755, 2007.

[98] Raghavachari, K., Trucks, G. W., Pople, J. A., and Head-Gordon, M., "A 5th-order perturbation comparison of electron correlation theories," *Chem. Phys. Lett.*, vol. 157, pp. 479–483, 1989.

[99] Rashkin, M. J. and Waters, M. L., "Unexpected substituent effects in offset π-π stacked interactions in water," *J. Am. Chem. Soc.*, vol. 124, no. 9, pp. 1860–1861, 2002.

[100] Reid, G. C. *Adv. At. Mol. Phys.*, vol. 12, p. 375, 1976.

[101] Rhee, Y. M., Lee, T. J., Gudipati, M. S., Allamandola, L. J., and Head-Gordon, M. *Proc. Natl. Acad. Sci. U.S.A.*, vol. 104, p. 5274, 2007.

[102] Riley, K. E. and Merz, K. M., "Effects of fluorine substitution on the edge-to-face interaction of the benzene dimer," *J. Phys. Chem. B*, vol. 109, pp. 17752–17756, 2005.

[103] Ringer, A. L., Sinnokrot, M. O., Lively, R. P., and Sherrill, C. D., "The effect of multiple substituents on sandwich and t-shaped π-π interactions," *Chem. Eur. J.*, vol. 12, pp. 3821–3828, 2006.

[104] Rodriguez-Monge, L. and Larsson, S. *J. Phys. Chem.*, vol. 100, p. 6298, 1996.

[105] Roncali, J., Leriche, P., and Cravino, A., "From one- to three-dimensional organic semiconductors: In search of the organic silicon," *Adv. Mater.*, vol. 19, p. 2045, 2007.

[106] Rowe, D. J. *Rev. Mod. Phys.*, vol. 40, p. 153, 1968.

[107] Russ, N. J., Crawford, T. D., and Tschumper, G. S. *J. Chem. Phys.*, vol. 120, p. 7298, 2005.

[108] S. A. Kucharski, M. Wloch, M. M. and Bartlett, R. J. *J. Chem. Phys.*, vol. 115, p. 8263, 2001.

[109] S. Hirata, M. N. and Bartlett, R. J. *Chem. Phys. Lett.*, vol. 328, p. 459, 2000.

[110] Saenger, W., *Principles of Nucleic Acid Structure*. New York: Springer-Verlag, 1984.

[111] Sekino, H. and Bartlett, R. J. *Int. J. Quant. Chem. Symp.*, vol. 18, p. 255, 1984.

[112] Shao, Y., Molnar, L. F., Jung, Y., Kussmann, J., Ochsenfeld, C., Brown, S. T., Gilbert, A. T. B., Slipchenko, L. V., Levchenko, S. V., O'Neill, D. P., Jr., R. A. D., Lochan, R. C., Wang, T., Beran, G. J. O., Besley, N. A., Herbert, J. M., Lin, C. Y., Voorhis, T. V., Chien, S. H., Sodt, A., Steele, R. P., Rassolov, V. A., Maslen, P. E., Korambath, P. P., Adamson, R. D., Austin, B., Baker, J., Byrd, E. F. C., Dachsel, H., Doerksen, R. J., Dreuw, A., Dunietz, B. D., Dutoi, A. D., Furlani, T. R., Gwaltney, S. R., Heyden, A., Hirata, S., Hsu, C.-P., Kedziora, G., Khalliulin, R. Z., Klunzinger, P., Lee, A. M., Lee, M. S., Liang, W., Lotan, I., Nair, N., Peters, B., Proynov, E. I., Pieniazek, P. A., Rhee, Y. M., Ritchie, J., Rosta, E., Sherrill, C. D., Simmonett, A. C., Subotnik, J. E., Woodcock, H. L., Zhang, W., Bell, A. T., Chakraborty, A. K., Chipman, D. M., Keil, F. J., Warshel, A., Hehre, W. J., Schaefer, H. F., Kong, J., Krylov, A. I., Gill, P. M. W., and Head-Gordon, M., "Advances in methods and algorithms in a modern quantum chemistry program package," *Phys. Chem. Chem. Phys.*, vol. 8, pp. 3172–3191, 2006.

[113] Shieh, H.-S., Berman, H. M., Dabrow, M., and Neidle, S., "The structure of drug-deoxydinucleoside phosphate complex; generalized conformational behavior of intercalation complexes with RNA and DNA fragments," *Nucleic Acids Res.*, vol. 8, pp. 85–97, 1980.

[114] Shkrob, I. A., Sauer Jr., M. C., Jonah, C. D., and Takahashi, K. *J. Phys. Chem. A.*, vol. 106, p. 11855, 2002.

[115] Simons, J. and Smith, W. D. *J. Chem. Phys.*, vol. 58, p. 4899, 1973.

[116] Sinha, D., Mukhopadhyay, D., Chaudhuri, R., and Mukherjee, D. *Chem. Phys. Lett.*, vol. 154, p. 544, 1989.

[117] Sinha, D., Mukhopadhyay, D., and Mukherjee, D. *Chem. Phys. Lett.*, vol. 129, p. 369, 1986.

[118] Sinnokrot, M. O. and Sherrill, C. D., "Unexpected substituent effects in face-to-face π-stacking interactions," *J. Phys. Chem. A*, vol. 107, pp. 8377–8379, 2003.

[119] Sinnokrot, M. O. and Sherrill, C. D., "Highly accurate coupled cluster potential energy curves for benzene dimer: The sandwich, t-shaped, and parallel-displaced configurations," *J. Phys. Chem. A*, vol. 108, no. 46, pp. 10200–10207, 2004.

[120] Sinnokrot, M. O. and Sherrill, C. D., "Substituent effects in π-π interactions: Sandwich and t-shaped configurations," *J. Am. Chem. Soc.*, vol. 126, pp. 7690–7697, 2004.

[121] Sinnokrot, M. O. and Sherrill, C. D., "High-accuracy quantum mechanical studies of π-π interactions in benzene dimers," *J. Phys. Chem. A*, vol. 110, pp. 10656–10668, 2006.

[122] Sinnokrot, M. O., Valeev, E. F., and Sherrill, C. D., "Estimates of the ab initio limit for π-π interactions: The benzene dimer," *J. Am. Chem. Soc.*, vol. 124, pp. 10887–10893, 2002.

[123] Slipchenko, L. V. and Krylov, A. I. *J. Chem. Phys.*, vol. 123, p. 84107, 2005.

[124] Slipchenko, L. V. and Krylov, A. I. *J. Phys. Chem. A*, vol. 110, p. 291, 2006.

[125] Smith, D. M. A., Rosso, K. M., Dupuis, M. V. M., and Straatsma, T. P. *J. Phys. Chem. B.*, vol. 110, p. 15582, 2006.

[126] Sodupe, M., Bertran, J., Rodriguez-Santiago, L., and Baerends, E. J. *J. Phys. Chem. A*, vol. 103, p. 166, 1999.

[127] Špirko, V., Engkvist, O., Soldán, P., Selzle, H. L., Schlag, E. W., and Hobza, P., "Structure and vibrational dynamics of the benzene dimer," *J. Chem. Phys.*, vol. 111, no. 2, pp. 572–582, 1999.

[128] Stanton, J. F. and Bartlett, R. J. *J. Chem. Phys.*, vol. 98, p. 7029, 1993.

[129] Stanton, J. F. and Gauss, J. *J. Chem. Phys.*, vol. 101, p. 8938, 1994.

[130] Stanton, J. F. and Gauss, J. *J. Chem. Phys.*, vol. 111, p. 8785, 1999.

[131] Swart, M., van der Wijst, T., Guerra, C. F., and Bickelhaupt, F. M. *J. Mol. Model.*, vol. 13, p. 1245, 2007.

[132] Szabo, A. and Ostlund, N. S., *Modern Quantum Chemistry*. McGraw-Hill, 1989.

[133] Tsuzuki, S., Honda, K., Uchimaru, T., and Mikami, M., "Intermolecular interactions of nitrobenzene-benzene complex and nitrobenzene dimer: Significant stabilization of slipped-parallel orientation by dispersion interaction," *J. Chem. Phys.*, vol. 125, p. 124304, 2006.

[134] Tsuzuki, S., Honda, K., Uchimaru, T., Mikami, M., and Tanabe, K., "Origin of attraction and directionality of the π-π interaction: Model chemistry calculations of benzene dimer interaction," *J. Am. Chem. Soc.*, vol. 124, no. 1, pp. 104–112, 2002.

[135] Tsuzuki, S., Uchimaru, T., Matsumura, K., Mikami, M., and Tanabe, K., "Effects of the higher electron correlation correction on the calculated intermolecular interaction energies of benzene and naphthalene dimers: comparison between MP2 and CCSD(T) calculations," *Chem. Phys. Lett.*, vol. 319, pp. 547–554, 2000.

[136] Tsuzuki, S., Uchimaru, T., Sugawara, K., and Mikami, M., "Energy profile of the interconversion path between t-shape and slipped-parallel benzene dimers," *J. Chem. Phys.*, vol. 117, no. 24, pp. 11216–11221, 2002.

[137] V. Polo, E. K. and Cremer, D. *Mol. Phys.*, vol. 100, p. 1771, 2002.

[138] V. Vanovschi, A. I. K. and Wenthold, P. G. *Theor. Chim. Acta*, vol. 120, p. 45, 2008.

[139] Werner, H. J. and Knowles, P. J. *J. Chem. Phys.*, vol. 89, p. 5803, 1988.

[140] Werner, H. J., Knowles, P. J., Lindh, R., Manby, F. R., Schütz, M., Celani, P., Korona, T., Rauhut, G., Amos, R. D., Bernhardsson, A., Berning, A., Cooper, D. L., Deegan, M. J. O., Dobbyn, A. J., Eckert, F., Hampel, C., Hetzer, G., Lloyd, A. W., McNicholas, S. J., Meyer, W., Mura, M. E., Nicklass, A., Palmieri, P., Pitzer, R., Schumann, U., Stoll, H., Stone, A. J., Tarroni, R., and Thorsteinsson, T., "MOLPRO, version 2006.1, a package of ab initio programs, see http://www.molpro.net.."

[141] Werner, H.-J., Manby, F. R., and Knowles, P. J., "Fast linear scaling second-order møller-plesset perturbation theory (MP2) using local and density fitting approximations," *J. Chem. Phys.*, vol. 118, no. 18, pp. 8149–8160, 2003.

[142] Werner, H. J. and Meyer, W. *J. Chem. Phys.*, vol. 74, p. 5802, 1981.

[143] Williams, H. L., Szalewicz, K., Jeziorski, B., Moszynski, R., and Rybak, S., "Symmetry-adapted perturbation theory calculation of the Ar-H_2 intermolecular potential energy surface," *J. Chem. Phys.*, vol. 98, pp. 1279–1292, 1993.

[144] Yang, C. H. and Hsu, C. P. *J. Chem. Phys.*, vol. 124, p. 244507, 2006.

[145] Yarkony, D. R. *J. Phys. Chem. A*, vol. 102, p. 8073, 1998.

[146] You, Z. Q., Shao, Y. H., and Hsu, C. P. *Chem. Phys. Lett.*, vol. 390, p. 116, 2004.

[147] Zhang, L. Y. and Friesner, R. A. *Proc. Natl. Acad. Sci.*, vol. 95, p. 13603, 1998.

[148] Zhang, Y. and Yang, W., "A challenge for density functionals: Self-interaction error increases for systems with a noninteger number of electrons," *J. Chem. Phys.*, vol. 109, pp. 2604–2608, 1998.